morphology in a BDNF-dependent manner. Therefore, considering that astrocytes modulate synaptic transmission (Bezzi *et al.*, 2004; Fiacco & McCarthy, 2004), these results indicate that the morphological changes regulated by the BDNF–T1 signal in astrocytes might play important roles in adult synaptic plasticity in the neocortex.

Materials and methods

T1 siRNA vector

The T1 siRNA vector was produced using the BLOCK-iT U6 Entry Vector kit (Invitrogen, Carlsbad, CA, USA). The pENTR/U6 vector integrates the human U6 promoter which drives RNA polymerase III. Generally, transcription by RNA polymerase III produces a higher amount of RNA than that by RNA polymerase II. Moreover, the U6 promoter belongs to a type III polymerase promoter, which is suitable for expressing a short-length RNA such as short hairpin RNA and micro RNA, for use in RNA interference because there is no internal promoter in it.

Briefly, 5′ oligo CAGCGTCATAAGATCCCCCTGGATGAGAATCCAGGGGGATCTTATGA and 3′ oligo AAAATCATAAGATCCCCCTGGATTCTCATCCAGGGGGATCTTATGAC were incubated at 95 °C for 4 min. The mixture was cooled to room temperature for 10 min to generate the double-strand oligo. The double-strand oligo was cloned into the pENTR/U6 vector. For the control oligos, 5′ oligo CAGCGAAGATCCCCCTGGATGGGAACGCCCATCCAGGGGGATCTT and 3′ oligo AAAAAAGATCCCCCTGGATGGGCGTTCCCATCCAGGGGGATCTTC were used.

Western blot analysis

C6 cells (Dainippon Pharmaceutical, Osaka, Japan) were maintained in Ham's F-10 medium (Gibco, Rockville, MD, USA) supplemented with 15% horse serum (Gibco) and 2.5% fetal bovine serum (Gibco) in a humidified atmosphere containing 5% CO_2 at 37 °C. The vectors (2 μg per 6-cm dish) were transfected into C6 cells (50% confluent) with FuGENE6 (Roche, Basel, Switzerland; Wiesenhofer *et al.*, 1999). The transfection efficiency of the green fluorescent protein (GFP) expression vector was ~ 60%. After 24 h, the cells were lysed in lysis buffer (Tris-HCl, pH 7.5, 50 mM; NaCl, 150 mM; $MgCl_2$, 5 mM; Triton X-100, 0.5%; PMSF, 1 mM; leupeptin, 10 μg/mL; and aprotinin, 20 μg/mL). After the lysed cells were centrifuged at 10 000 ***g*** at 4 °C for 20 min, the supernatants were mixed with 4 × sodium dodecyl sulphate (SDS) sample buffer and boiled for 3 min. Samples (5 μg/lane for actin and tubulin, 100 μg/lane for T1) were subjected to SDS–polyacrylamide gel electrophoresis (7% gel for T1, 12% gel for actin and tubulin), and the proteins were blotted onto polyvinylidene difluoride membranes (Millipore, Billerica, MA, USA). The membranes were blocked in 5% skimmed milk in phosphate-buffered saline (PBS; in mM: NaCl, 137; Na_2HPO_4, 8.1; KCl, 2.7; and KH_2PO_4, 1.5). After incubation of the blots with antibodies (anti-T1, diluted at 1 : 200; Santa Cruz Biotech., Santa Cruz, CA, USA; antiactin, diluted at 1 : 200; and antitubulin, diluted at 1 : 200; both Sigma, St Louis, MO, USA) at room temperature for 1 h, they were incubated with secondary antibodies conjugated with horseradish peroxidase and the proteins were visualized by the enhanced chemiluminescence system (Amersham Pharmacia Biotech, Tokyo, Japan). The specificity of anti-T1 antibody for use with Western blot analysis and immunohistochemistry has already been assessed in our previous studies (Ohira *et al.*, 1999; Ohira & Hayashi, 2003). For the quantitative analysis of protein bands we measured the band areas using ImageJ software.

Electroporation

The methods were approved by the National Institute of Neuroscience Committee for the Ethical use of Experimental Animals, based on the guiding principles of the Council for International Organizations of Medical Sciences (1984). Every effort was made to minimize the number of animals used. Adult male Sprague–Dawley (S-D) rats (4–6 weeks, $n = 10$) were deeply anaesthetized with sodium pentobarbital (50 mg/kg). A rectangular hole in the right hemisphere of the skull (3 mm wide and 5 mm long) was created. After an anode tungsten needle was stereotaxically and diagonally inserted under the neocortex (2 mm posterior and 3.5 mm lateral to the bregma, at an angle of 20° to the brain surface), a mixture of 20 μL (GFP : siRNA, 1 : 5) of GFP plasmid vector solution (pCA-GFP; 1 μg/μL in 0.01% Fast Green in Tyrode's solution) and T1 siRNA (1 μg/μL) or the control vectors (1 μg/μL) was injected between the arachnoid and the dura using a pipette (P-20; Gilson, Middleton, WI, USA) connected to a silicon tube and a 27-gauge injection needle (Terumo, Tokyo, Japan). The rectangular platinum plate cathode (1 mm wide and 1.5 mm long) was placed on the dura, and a series of five square pulses (50 ms, 15 V, 950-ms intervals) were immediately sent using Electro Square Porator model T820 and Optimizor 500 (BTX, Harvard Apparatus, Holliston, MA, USA). At 3 days after electroporation, the rats were killed and the brains were removed in order to prepare acute slices.

Morphological assay

Rats were anaesthetised with pentobarbital sodium (25 mg/kg i.p.). After decapitation, the brains were removed from normal (4–6 weeks S-D rat, $n = 10$) and electroporated rats (4–6 weeks S-D rat, $n = 10$) and yellow fluorescent protein (YFP) transgenic mice [4–6 weeks, $n = 3$; B6.Cg-Tg (Thy1-YFP) 16Jrs/J, The Jackson Laboratory, Bar Harbor, ME, USA], and 500-μm slices were created. The slices were kept for 30 min at 4 °C in DMEM (Invitrogen, Carlsbad, CA, USA) containing N2 supplement (Invitrogen). For the administration of reagents, the slices were stimulated for 60 min at 37 °C and 5% CO_2 with 20 ng/mL BDNF (PeproTech, Rocky Hill, NJ, USA) or 100 ng/mL NGF (PeproTech). The dishes were agitated gently during incubation. Then, the slices were fixed at 4 °C for 1 h in 4% PFA in PBS. For cryoprotection, they were sequentially immersed in 5, 10, 20 and 30% sucrose. Thereafter, the slices were further sliced into 10-μm-thick sections and were incubated with the primary antibodies at 4 °C for 48 h. For the double staining analysis, we used the following primary antibodies: the rabbit polyclonal antibodies were antiglial fibrillary acidic protein (GFAP; diluted at 1 : 50; Sigma) and anti-T1 (diluted at 1 : 1600; Santa Cruz Biotech.); and the mouse monoclonal antibodies were antiglutamic acid decarboxylase 65/67 (diluted at 1 : 10 000; Affinity Research Products, Exeter, UK), anti-GFAP (diluted at 1 : 1000; Chemicon, Temecula, CA, USA), and antisynaptophysin (diluted at 1 : 1000; Chemicon). For the T1 staining procedure, in order to retrieve antigenicity the samples were preincubated in 6 M guanidine chloride in 50 mM Tris-HCl, pH 10.2, for 15 min at room temperature (Ohira *et al.*, 2003, 2004, 2005a, 2005b). For the morphological analyses of the astrocytes, the parameters were defined as follows: a thick process that extended radially from a soma was defined as a primary process, and a fine process that extended from a primary process was designated a branch. For the analysis of synaptophysin-positive ($^+$) sites, the number of sites per 14 500 μm^2 was counted. For the analysis of the interaction among synaptophysin$^+$ sites and GFAP$^+$ processes, the number of synaptophysin$^+$ sites that were piled on (white in Fig. 6A and B) or contacted with GFAP$^+$ processes (blue in Fig. 6A and B) was counted

in an area of 14 500 μm^2. The samples in a 0.5-μm-thick plane were analysed using a confocal microscope (TCS SP2; Leica, Wetzlar, Germany). In this assay, we chose the layer I areas to be analysed at random.

For the quantitative analysis of *in vivo* fluorescent intensity of T1, the images of astrocytes were taken under the same condition. Fluorescent intensity was measured with ImageJ software.

Terminal deoxynucleotidyl transferase-mediated digoxigenin nucleotide nick-end labelling (TUNEL) staining

Apoptotic cells were identified by using modified ApopTag apoptosis detection systems (Serologicals, Norcross, GA, USA). For the analyses of injured cortices, young adult male S-D rats (4–6 weeks, $n = 3$) were deeply anaesthetized with sodium pentobarbital (50 mg/kg). Rectangular holes were bored into the skull (3 mm wide and 5 mm long) over the right hemisphere. The motor cortex was injured by the application of a surgical knife attached to the tip of the vertical bar of the stereotaxic instrument; this procedure was performed according to the stereotaxic brain atlas (Paxinos & Watson, 1986). The stereotaxic coordinates used for cutting were as follows: anteroposterior, +1 to −1.5 mm from bregma; lateral, 4 mm from the midline; and depth, 1 mm below the brain surface. At 2 days after the operation, the brains were fixed in 4% PFA. The brain sections (10 μm) from the injured and electroporated rats were incubated with terminal deoxynucleotidyl transferase for 1 h at 37 °C. Thereafter, the sections were stained with antidigoxigenin (Roche Applied Science, Basel, Switzerland) and with secondary antibody conjugated with Cy3 (Chemicon). Nuclei were stained with Hoechst 33258 (Sigma).

Data collection

In the following two analyses (the astrocytic morphology and the relationship between $GFAP^+$ processes and $synaptophysin^+$ sites), we obtained the data from 10 normal rats, five control vector-electroporated rats and five T1 siRNA vector-electroporated rats. In addition, one control and one siRNA vector-electroporated rat was subjected to each analysis.

In order to analyse astrocytic morphology, we collected data from 57 cells in normal slices not treated with BDNF, 63 cells in normal slices treated with BDNF, 62 cells in normal slices not treated with NGF, 60 cells in normal slices treated with NGF, 71 cells in control vector-electroporated slices not treated with BDNF, 75 cells in control vector-electroporated slices treated with BDNF, 71 cells in siRNA vector-electroporated slices not treated with BDNF and 66 cells in siRNA vector-electroporated slices treated with BDNF. For the analysis of the relationship between $GFAP^+$ processes and $synaptophysin^+$ sites, the data was obtained from the following: 44 normal sections not treated with BDNF, 47 normal sections treated with BDNF, 43 normal sections not treated with NGF, 45 sections treated with NGF, 47 control vector-electroporated sections not treated with BDNF, 46 control vector-electroporated sections treated with BDNF, 49 siRNA vector-electroporated sections not treated with BDNF and 48 siRNA vector-electroporated sections treated with BDNF.

Results

BDNF-dependent morphological change in astrocytes in neocortical layer I of acute slices prepared from adult rats

Astrocytes in the CNS are generally divided into two groups, fibrous and protoplasmic astrocytes. Fibrous astrocytes are characterized by (i) long processes with slight branching, (ii) GFAP-rich contents and (iii) distribution in the white matter and in neocortical layer I. Protoplasmic astrocytes have the following typical features: (i) well-branching short processes, (ii) low GFAP content and (iii) distribution in the grey matter (Peters *et al.*, 1976; Raff *et al.*, 1983; Miller & Raff, 1984). In the present study an immunofluorescent approach was used to observe layer I fibrous astrocytes, but the protoplasmic astrocytes in layers II–VI were not observed. As GFAP was observed in large amounts in the layer I fibrous astrocytes, a double-immunofluorescence study of GFAP and T1 enabled the visualization of layer I fibrous astrocytes (Fig. 1A). Also, the layer I fibrous astrocytes do not overlap their neighbours' space (Fig. 2). Similarly, the protoplasmic astrocytes in hippocampal CA1 stratum radiatum have separate domains (Bushong *et al.*, 2002). Therefore, we were able to observe individual astrocytes without any intermingling. Moreover, in our preliminary study we visualized the morphology of astrocytes in neocortical layer I of acute brain slices prepared from developing mice (postnatal days 14–20) using a combination of intracellular recording, biocytin injection and coimmunofluorescent staining with GFAP. These findings were in contrast to those obtained with protoplasmic astrocytes, in which GFAP only enables the visualization of ~15% of the total cell volume in the hippocampal CA1 (Bushong *et al.*, 2002). The layer I astrocytes exhibited a mean resting membrane potential of −77.3 ± 7.0 mV (total $n = 8$ cells), and did not produce action potentials. The morphology revealed by biocytin injection into glial cells that had been electrophysiologically identified was consistent with that of neocortical layer I astrocytes in adult mammals (Colombo *et al.*, 2000). Although this intracellular staining method could reveal the morphology of astrocytes clearly in the developing cortex by 3 weeks postnatal, it was impracticable to make whole-cell patch-clamp recordings of astrocytes in adult slices of mice and rats. Our aim of this study was to determine whether T1 was involved in the regulation of morphological changes in astrocytes in the adult cortex. In this study, therefore, whole-cell patch-clamp recording was abandoned in favour of investigating the morphological changes in astrocytes in the adult cortex. In our rat preparation, a double-immunofluorescence study of GFAP and T1 expression revealed that the cell shape of neocortical layer I astrocytes was quite similar to that observed in the mouse preparation. The length of layer I astrocytes in our study (mean ± SD, 24.5 ± 9.2 μm; total, 194 processes from 57 astrocytes) was similar to the data reported by Colombo *et al.*, 2000). Thus, we concluded that the cell shape observed in the double-immunofluorescence study with GFAP and T1 probably reflects the actual cell bodies and processes of the astrocytes in layer I. We therefore focused on layer I fibrous astrocytes.

As shown in Fig. 1, we observed rapid morphological changes among layer I astrocytes with BDNF treatment for 1 h. BDNF treatment induced process elongation and branching, but it did not lead to an increase in the number of primary processes from each soma. In contrast, NGF treatment had no effect on astrocytic morphological changes. Together with the finding that the layer I astrocytes express mainly T1 *in vivo* (Ohira *et al.*, 2005a), this finding regarding morphological changes among astrocytes is suggestive of an induction by the T1 signalling cascade in the astrocytes themselves.

Effect of T1 siRNA on astrocytic morphology

Next, in order to examine the contribution of T1 to BDNF-dependent morphological changes in astrocytes, we constructed T1 siRNA-expression vectors. Then, using rat glioma C6 cells that intrinsically express T1, we confirmed the RNA interference effect of this vector (Fig. 3). At 24 h after transfection, the expression level of T1 had not changed in the control vector-transfected cells (Fig. 3B). On the other

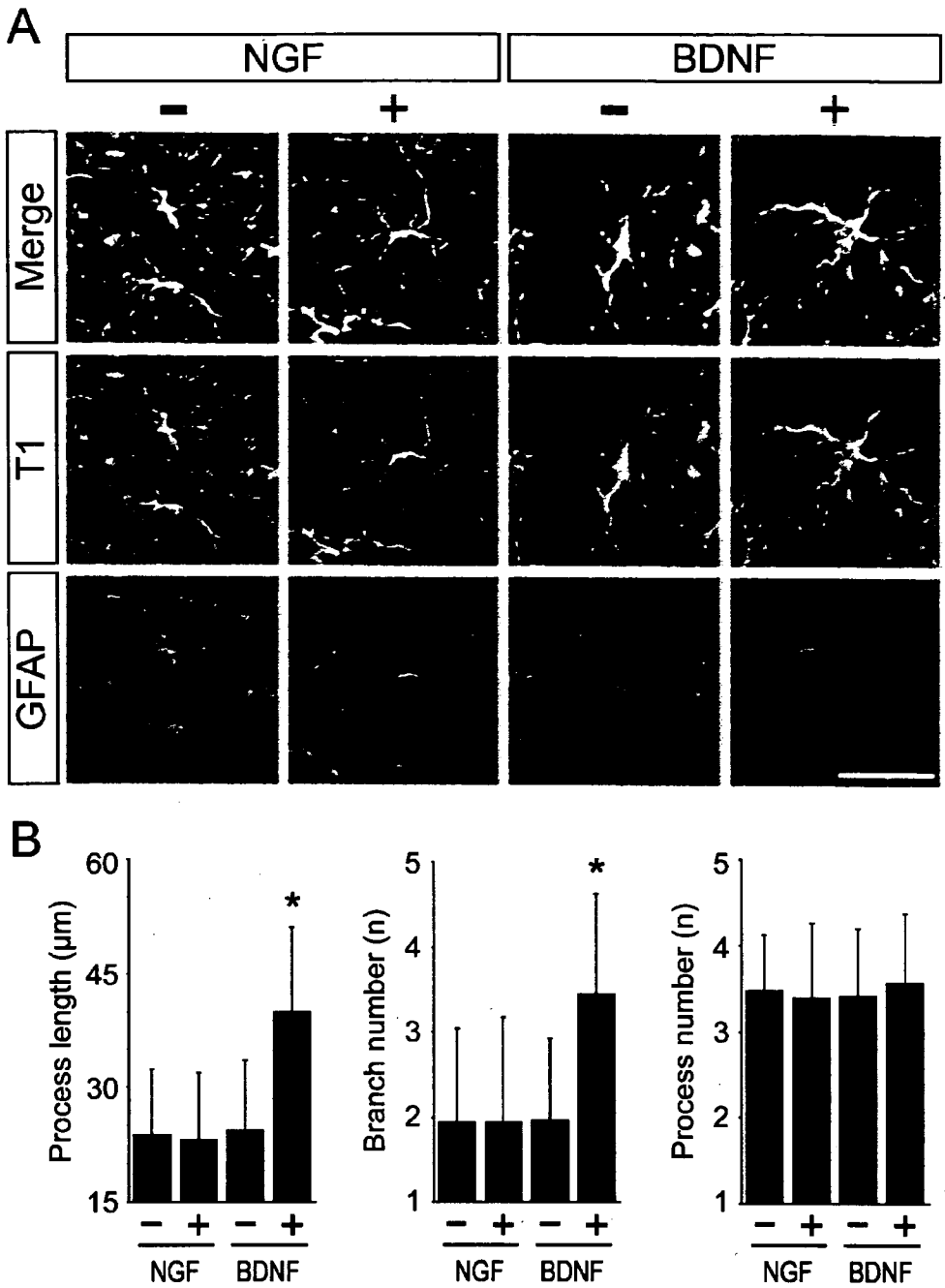

FIG. 1. Morphological changes in astrocytes. (A) Astrocytes in layer I of the motor cortex were stained by anti-T1 (blue) and anti-GFAP (red). (B) Quantitative analyses of process length (left panel), number of branches (middle panel) and number of processes (right panel). Values are given as means ± SD and are the results of four independent experiments. $*P < 0.05$ (one-way ANOVA and Scheffé's *post hoc* test) compared to the astrocytes in slices not treated with BDNF; −, no stimulation; +, stimulation with NGF or BDNF. Scale bar, 30 μm.

hand, in the T1 siRNA-transfected cells, T1 expression was decreased to 1/4 of the control level (Fig. 3B). Thus, we concluded that the T1 siRNA-expression vectors were effective at suppressing the expression of T1 proteins.

In order to deliver the T1 siRNA-expression vectors into the layer I astrocytes, we performed an electroporation of T1 siRNA-expression vectors into the neocortex of living rats. At 3 days after electroporation, the neocortical slices were subjected to a series of morphological analyses. The vectors were focally electroporated into layer I cells, such that we did not observe GFP expression in neurons and glial cells of layers II–VI. As this *in vivo* electroporation damaged brain tissue under the cathode plate, for this analysis we chose regions in which there were neither apoptotic nor necrotic cells in the electroporated tissues (Fig. 4). As a positive control for the TUNEL method we used brain tissues damaged with a surgical knife. In the control sections, apoptotic cells were observed (Fig. 4A–C), while there were no apoptotic cells in the neighbouring sections subjected to the morphological analysis of astrocytes (Fig. 4G–N). At the same

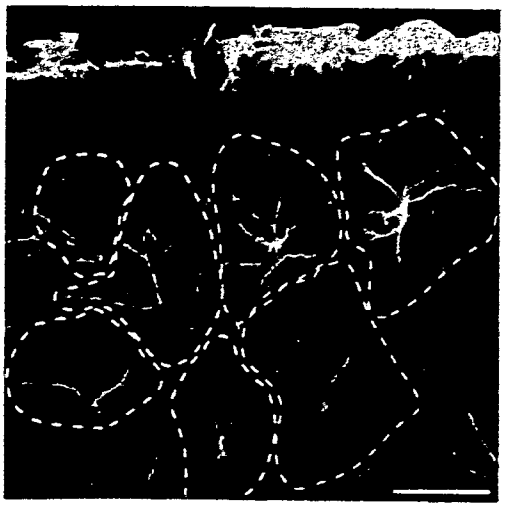

FIG. 2. Individual domains of layer I fibrous astrocytes. Astrocytes were visualized with anti-GFAP (green). The white dotted lines indicate the domain of each layer I fibrous astrocyte. Note that layer I fibrous astrocytes have separate domains, suggesting that we can observe the fine structures of astrocytes, such as processes and branching, without the problems of intermingling. Scale bar, 25 μm.

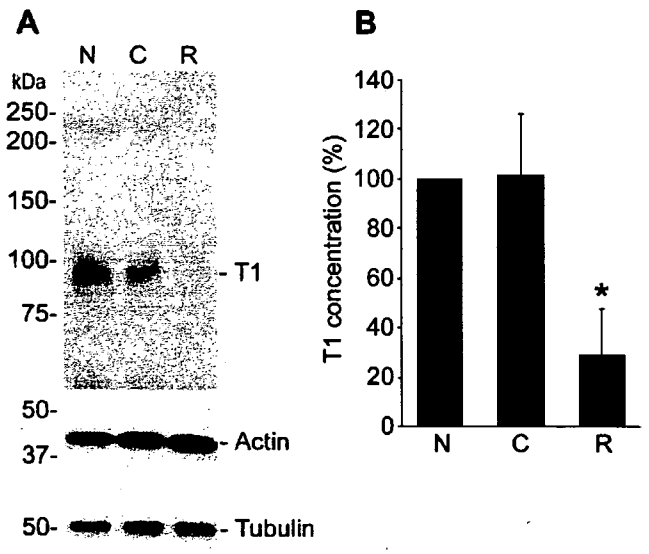

FIG. 3. Effect of T1 siRNA on T1 expression in C6 cells. (A) Either control vectors or T1 siRNA-expression vectors were transfected into C6 cells that intrinsically express T1. The expression of T1 was examined by Western blot analysis with anti-T1. The molecular weight of T1 was 95 kDa. The positions of the molecular weight markers are shown on the left. (B) Quantitative analysis of T1 bands in A. The expression level of T1 in the no transfection sample was taken as 100%. $*P < 0.05$ (one-way ANOVA) compared to the level of the no transfection sample. Values are given as means ± SD and were obtained from three independent experiments, and a representative image is shown. N, no transfection; C, control vector; R, siRNA vector.

time we assumed that the T1 siRNA-expression vector had been transferred into the astrocytes; this assumption was based on the expression of GFP, the expression vector of which was cotransferred with the siRNA vectors. In addition, it was observed that the GFP-expressing astrocytes did show a reduction in the T1 expression level (panel T1 in Fig. 5A).

To determine the *in vivo* efficiency of T1 siRNA, the quantitative analysis of *in vivo* T1 expression in the control- or siRNA-vector electroporated astrocytes was performed by measuring the fluorescent intensity of T1. The fluorescent intensity of T1 in the siRNA vector-electroporated astrocytes was significantly decreased compared with that in the control vector-electroporated astrocytes (Fig. 5C). Therefore, based on T1 expression, the siRNA vector was effective.

In the slices prepared from control vector-electroporated rats, BDNF induced a significant increment in the length and number of branches of the processes, while no change in primary process number was observed (Fig. 5). These amounts of change were identical to those observed in the nonelectroporated slices (Figs 1 and 5). When not treated with BDNF, slices prepared from the T1 siRNA vector-electroporated rats showed no difference from those with control vectors. Also, the astrocytes containing T1 siRNA-expression vectors appeared to have fewer branches and shorter processes under the no-BDNF treatment condition, though this difference was not significant (Fig. 5B). This result might be caused by an increase in cytosolic Rho GTPases due to the reduced expression of T1, which might bind and retain Rho GDI1 in the cell membrane. When treated with BDNF and inhibited T1 expression, astrocytes exhibited slight, albeit not significant, elongation and branching of the processes (Fig. 5B). These slight increases in process length and branching might be due to the low level of T1.

Relationship of GFAP$^+$ processes and synaptophysin$^+$ sites

Morphological changes in astrocytes have effects on the clearance of neurotransmitters and the regulation of synaptic transmission (Theodosis & Poulain, 1993; Iino *et al.*, 2001; Oliet *et al.*, 2001; Theodosis *et al.*, 2004). Moreover, in the cerebellum, Bergmann glial cells receive glutamate via ectopic release, and functional AMPA receptors are densely distributed in the Bergmann glial membrane that faces the synaptic structures (Matsui *et al.*, 2005), suggesting that astrocytic processes in close proximity to synapses may be capable of locally regulating synaptic functions. Thus, in this study we also addressed the question of whether or not the BDNF–T1 signalling leads to an increase in the number of synapses that are in contact with GFAP$^+$ processes. In this analysis, there is the possibility that synaptophysin$^+$ sites might represent cut axonal fibres. We assessed this problem using YFP-transgenic mice. In these mouse brains, YFP proteins were strongly expressed in the cell body, axons and dendrites of the layer V pyramidal neurons (Feng *et al.*, 2000). If cut axonal fibre terminals (YFP$^+$) were also synaptophysin$^+$, we would have detected the synaptophysin and YFP double-positive sites. However, we hardly found any such double-positive sites. Therefore, we considered synaptophysin$^+$ sites to be actual mature synapses (Okabe *et al.*, 2001). As shown in Fig. 6A and C, the number of synaptophysin$^+$ sites in contact with GFAP$^+$ processes increased in a BDNF-dependent manner, presumably because of the BDNF-induced extension of the astrocytic processes and astrocytic branching. On the other hand, neither BDNF nor NGF treatment was found to influence the overall density of synaptophysin$^+$ sites (Fig. 6D).

Next, we examined the effect of T1 siRNA on the interaction between GFAP$^+$ processes and synaptophysin$^+$ sites. In the control vector-electroporated slices, the number of synaptophysin$^+$ sites that were in contact with GFAP$^+$ processes increased more than two-fold, a result which was compatible with the amounts in the nonelectroporated slices (Fig. 6C). In contrast, no morphological changes among the astrocytes were observed in the T1 siRNA-expression vector electroporated slices. Moreover, the reduction in the number of synaptophysin$^+$ sites in contact with GFAP$^+$ processes appeared to

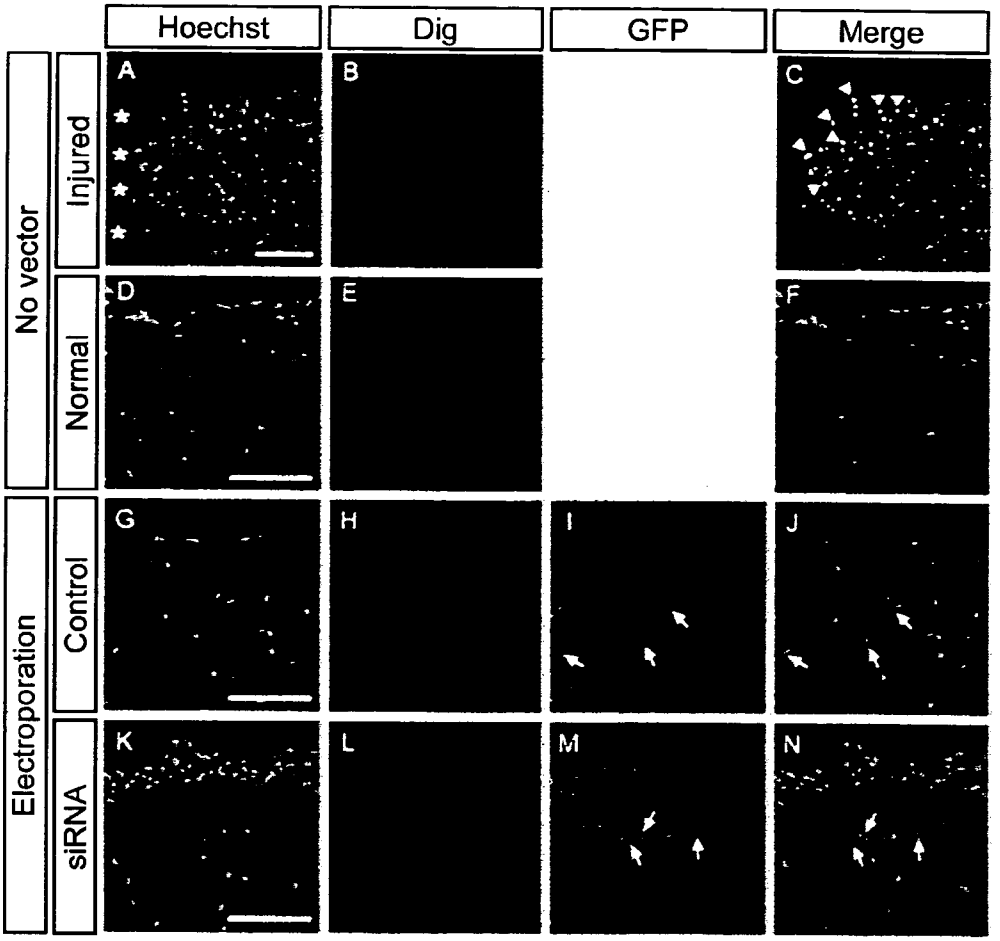

FIG. 4. Apoptotic cells in (A–C) injured, (D–F) unelectroporated, (G–J) control vector-electroporated, and (K–N) T1 siRNA vector-electroporated slices of the motor cortex. Apoptotic cells were detected by the TUNEL method with anti-Dig (B, E, H and L; red) and these cells are indicated by arrowheads. Electroporated cells expressed GFP (I and M; green cells indicated by arrows). Nuclei were stained with Hoechst 33258 (A, D, G, and K; blue). Note that the apoptotic cells, indicated by the arrowheads in C, were distributed around the injured region (asterisks in A), but were hardly detected in (E) the normal slices and in (H and L) the electroporated slices, thus suggesting that in these regions electroporation successfully delivered the plasmid vectors into neocortical layer I without inducing cell death. Scale bars, 100 μm.

reflect a decrease in $GFAP^+$ process length and in the branching induced by T1 siRNA, although this result was not significant (Fig. 6C).

Discussion

In this study, we demonstrated that BDNF regulated astrocytic morphology in adult neocortical slices via a truncated TrkB receptor, T1. Our data also revealed that the number of $synaptophysin^+$ sites in contact with $GFAP^+$ processes increased in a BDNF–T1-dependent manner without a change in the number of total $synaptophysin^+$ sites. Therefore, these results show that the neocortical layer I astrocytes exhibit high morphological plasticity in the adult rat brain.

Knock-down of T1 expression by siRNA and electroporation

In the present study, we performed *in vivo* knock-down of T1 by using T1 siRNA. The *trkB* gene contains at least three subtypes that have in common an extracellular domain, a transmembrane domain and the first 12 intracellular amino acid sequences. We designed the 19-mer oligonucleotide from adenosine at 1852 in the T1 sequence (GenBank accession number M55292). Interestingly, the control sequence started four nucleotides upstream of the T1 siRNA sequence. This control vector had virtually no RNAi effect on T1 expression (Fig. 3) or morphological changes in astrocytes (Figs 5 and 6), which was similar to the data from the normal rats (Figs 1 and 6). Although the cause was unknown, there was no great difference between the percentages of GC content in the two sequences. Thus, the secondary and/or tertiary structure of the resulting RNA might be the reason.

In this study, we performed electroporation to transfect the T1 siRNA-expression vectors into astrocytes. However, the electroporation and the cutting of slices kill the cells or weaken them. To choose the healthy areas in the slices, we checked the adjacent sections by the TUNEL method, which detects apoptotic cells. Also, we found gliosis as well as apoptosis at the margins of the areas damaged by electroporation. However, there was no gliosis in other areas (data not shown), because the electroporation of weak electric potential used in this study (five pulses of 50 ms, 15 V at 950-ms intervals) would cause limited focal damage, as reported in the previous studies (Kondoh *et al.*, 2000; Kachi *et al.*, 2005). Moreover, in the control vector-electroporated slices, the morphology of astrocytes (length,

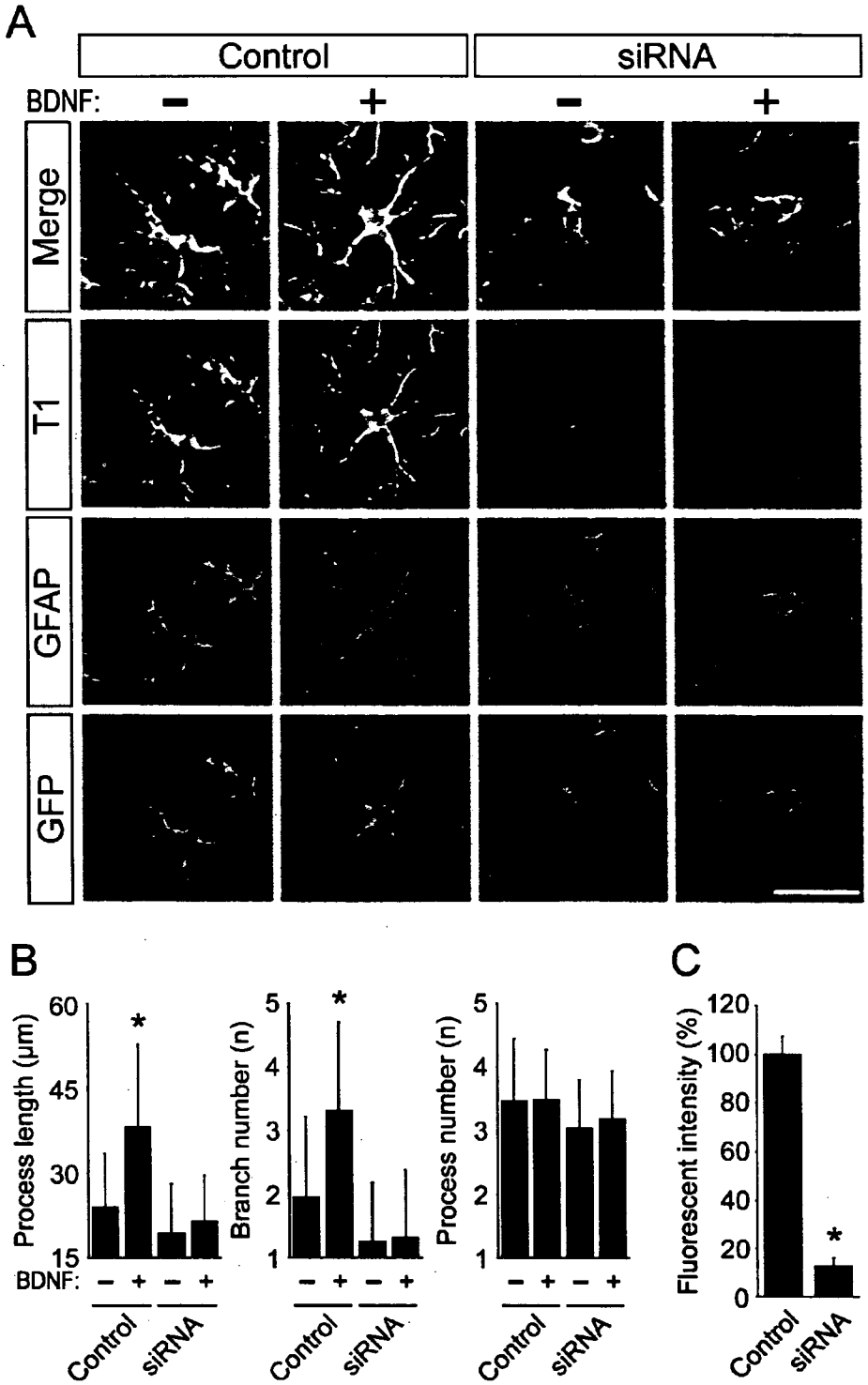

FIG. 5. Morphological changes in astrocytes transfected with T1 siRNA-expression vector. (A) Control or T1 siRNA-expression vector-electroporated astrocytes were visualized with anti-T1 (blue), anti-GFAP (red) and electroporated GFP (green). Slices were incubated for 60 min with BDNF (20 ng/mL) or vehicle (DMEM). Note that few T1-immunoreactive structures were observed in the T1 siRNA-expression vector-electroporated cells. (B) Quantitative analyses of process length (left panel), number of branches (middle panel) and number of processes (right panel). Values are given as means ± SD and are the results of four independent experiments. $*P < 0.05$ (two-way ANOVA) compared to astrocytes in the control slices not treated with BDNF. There was a significant difference in the BDNF treatment, but not a difference between the control- and the siRNA-expression vectors. (C) Quantitative analysis of T1 fluorescence intensity. Fluorescence intensity was measured with ImageJ. The expression level of T1 in the no transfection sample was taken as 100%. Values are given as means ± SD and are the results of four independent experiments. $*P < 0.05$, Student's *t*-test, between the T1 fluorescence intensity levels of the control and siRNA-expression vector transfected astrocytes. Control, electroporation of control vector; siRNA, electroporation of T1 siRNA-expression vector, –, no stimulation; +, stimulation with BDNF. Scale bar, 20 μm.

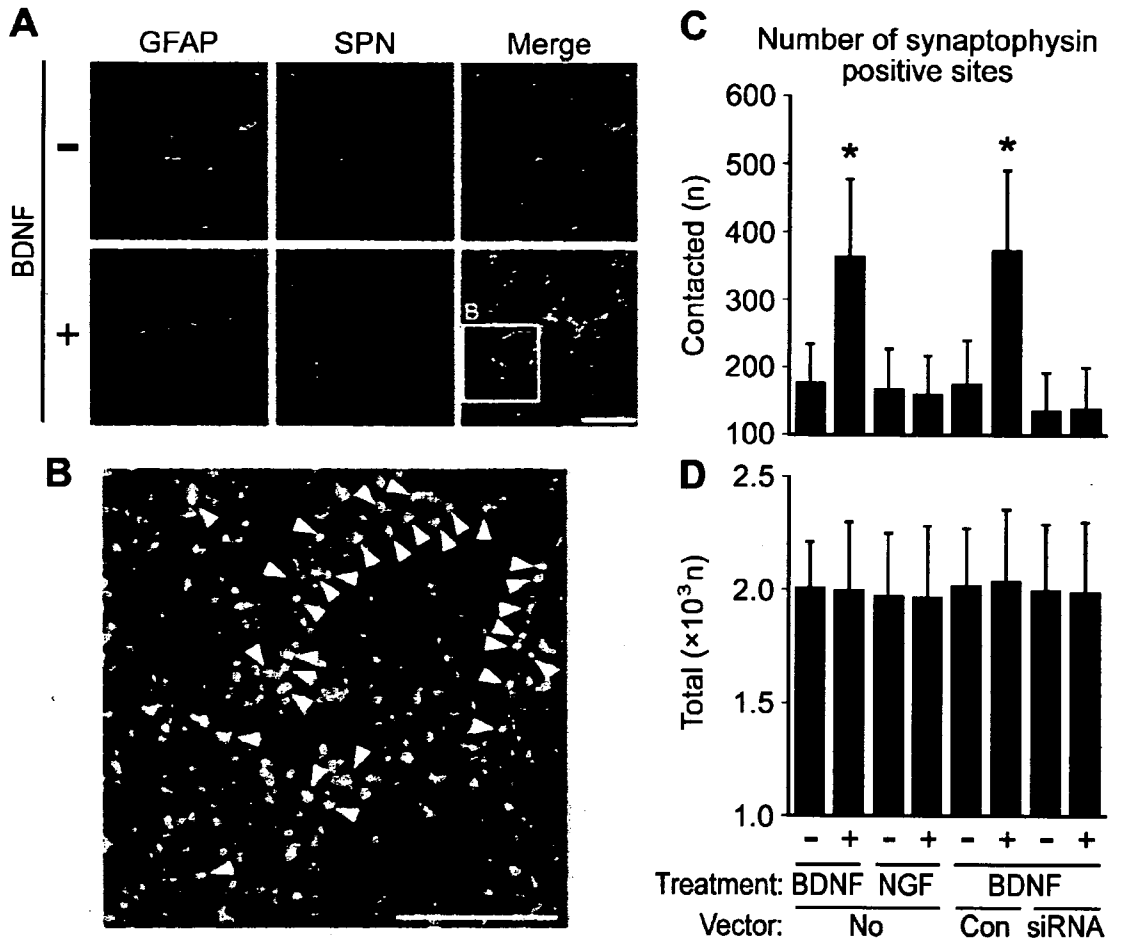

FIG. 6. Interaction between GFAP$^+$ processes and synaptophysin$^+$ sites. (A) Images of GFAP$^+$ processes (red) and synaptophysin (SPN)$^+$ sites (blue) in layer I of the motor cortex of normal acute slices. Slices were incubated for 60 min with BDNF (20 ng/mL) or vehicle (DMEM). (B) A high-powered image of the boxed-in area in A. Arrowheads indicate SPN$^+$ sites (white) in contact with GFAP$^+$ processes. (C and D) Quantitative analysis of (C) SPN$^+$ sites (white) in contact with GFAP$^+$ processes and (D) total SPN$^+$ sites. The normal slices, the control vector-electroporated slices and the RNAi vector-electroporated slices were treated with the indicated reagents: NGF (100 ng/mL), BDNF (20 ng/mL) and vehicle (DMEM). Values are given as means ± SD and are the results of four independent experiments. *P < 0.05 (one-way ANOVA and Scheffé's *post hoc* test) compared to the levels observed in astrocytes in normal slices not treated with BDNF; –, no stimulation; +, stimulation with NGF or BDNF. Scale bars, 20 μm.

branching and number of processes) was similar to that from the nontreated slices. Therefore, the morphology of astrocytes in the analysed areas was not affected by electroporation.

Subcellular localization of T1 and GFAP

The subcellular localization of T1 was very similar to that of GFAP (Figs 1 and 5). The single staining for T1 shows a uniform distribution of T1 in cell bodies and processes (Ohira *et al.*, 2005b). On the other hand, GFAP was also uniformly localized in the astrocytic cell bodies and processes (Fig. 2), suggesting that each specific antibody used here is not cross-reactive. Thus, these results indicate that proteins of both T1 and GFAP were distributed close to each other in astrocytes.

The colocalization of T1 and GFAP may indicate that T1 interacts with GFAP. In a previous study, we reported that T1 binds directly Rho GDI1, which is a negative regulator of a small G-protein family, Rho (Ohira *et al.*, 2005a). Additionally, T1 downregulates the activity of ROCK, a downstream effector kinase of RhoA, in a BDNF-dependent manner (Ohira *et al.*, 2006). Moreover, ROCK phosphorylates GFAP, which causes depolymerization of GFAP (Kosako *et al.*, 1997). Thus, T1 can regulate GFAP assembly via the Rho signalling pathway. Interestingly, all Trk family proteins can directly interact with an intermediate filament, peripherin (MacDonald *et al.*, 1999). All together, neurotrophins may be involved in regulation of cell morphology via cytoskeletal proteins such as intermediate filaments as well as microfilaments and microtubules (Etienne-Manneville & Hall, 2002).

Regulation of astrocytic morphology by BDNF–T1

In the adult mammalian CNS, BDNF is synthesized and secreted from pre- and postsynaptic neurons in a manner that depends on neuronal activity (Fawcett *et al.*, 1997, 1998; Aloyz *et al.*, 1999; Hartmann *et al.*, 2001; Kohara *et al.*, 2001). However, the physiological function of BDNF in the adult CNS remains unclear. One of the reasons that the function of BDNF in the adult mammalian CNS has not yet been clarified is that the function of T1, the major receptor for BDNF in the adult mammalian CNS from mice to nonhuman primates, has yet to be

addressed (Allendoerfer *et al.*, 1994; Fryer *et al.*, 1996; Ohira *et al.*, 1999). In the adult monkey prefrontal cortex, TK+/TK– heterodimers and TK–/TK– homodimers are formed in a BDNF-dependent manner; however, TK+/TK+ homodimers that function during development are not observed (Ohira *et al.*, 2001). These lines of evidence suggested that TK– (i.e. T1 in the adult neocortex) plays an important role in the maintenance and plasticity of the adult neocortex. Indeed, recent studies have demonstrated the function and signalling pathway of T1 (Rose *et al.*, 2003; Ohira *et al.*, 2005a; Ohira *et al.*, 2006). Thus, these studies provide clues to the elucidation of *in vivo* function of BDNF in the mature CNS.

T1 is expressed in both neurons and glial cells (Armanini *et al.*, 1995; Ohira *et al.*, 2005b), and it is highly involved in the regulation of the morphology of both types of cell (Yacoubian & Lo, 2000; Ohira *et al.*, 2005a). In terms of function, glial cells, and especially astrocytes, have been thought to play only a supportive role for neurons. However, recent studies have demonstrated that glial cells regulate the clearance of neurotransmitters, and that they maintain neural plasticity by themselves undergoing morphological changes (Theodosis & Poulain, 1993; Iino *et al.*, 2001; Oliet *et al.*, 2001; Theodosis *et al.*, 2004). In contrast, neuronal morphology in the adult rodent neocortex has been shown to be more static than previously thought (Grutzendler *et al.*, 2002). The findings of the present study are thus consistent with these previous findings. In the adult CNS, BDNF release might induce morphological changes in those astrocytic processes surrounding synapses via the T1 signalling pathway, eventually leading to rapid changes in synaptic strength and transmission (Wenzel *et al.*, 1991). However, it remains unclear whether or not the site-specific release of BDNF regulates astrocytic morphology and affects synaptic transmission and plasticity *in vivo* as well as in tissue slices.

It is reasonable to expect that BDNF treatment induces neurons to release factors that in turn regulate astrocytic morphology. In this study, we did not directly test this possibility. However, considering that (i) T1 regulates astrocytic morphology in astrocyte primary cultures in which the *in vivo* expression pattern of BDNF receptors is maintained (Ohira *et al.*, 2005a), and (ii) T1-specific siRNA electroporated into astrocytes suppressed BDNF-induced morphological changes in astrocytes, we concluded that the astrocytic morphology in the acute slices observed here was regulated by the BDNF–T1 signalling pathway in the astrocytes themselves.

In the present study, $GFAP^+$ astrocytic processes exhibited BDNF-dependent elongation of up to 15 μm, whereas previous studies have reported changes in process length of only several micrometers in the astrocytes of the brainstem (Hirrlinger *et al.*, 2004) and hippocampus (Benediktsson *et al.*, 2005). Previous reports have noted the spontaneous elongation and retraction of fine processes of protoplasmic astrocytes, in which glutamate, ATP and other factors would be expected to be involved in the regulation of astrocytic morphology (Volterra & Meldolesi, 2005). As *in vivo* BDNF release from synapses is regulated by neuronal activity, a bath application of BDNF would be expected to continuously stimulate astrocytes and result in a stronger elongation and branching effect among astrocytic processes. However, this effect may also reflect a difference between protoplasmic and fibrous astrocytes.

Functional significance of BDNF–T1 in neocortical layer I astrocytes

It is of note that, in the adult rat neocortex, the strongest BDNF immunoreactivity is observed in layer I (Yan *et al.*, 1997), which suggests that BDNF is enriched and functions in neocortical layer I. Neocortical layer I contains a small number of neurons and is composed predominantly of dendritic and axonal connections (Lund & Wu, 1997) which receive feedback inputs from the cortex (Rockland & Virga, 1989) and inputs from the thalamic nuclei (Glenn *et al.*, 1982; Lachica & Casagrande, 1992) as well as from other subcortical regions (Tigges & Tigges, 1985). The apical dendrites of pyramidal neurons in layers II–VI reach layer I (Lund & Wu, 1997). Thus, layer I is an important region in which the feedforward and feedback information from higher cortical areas, as well as from other lower cortical areas and subcortical regions, could be associated (Zhu & Zhu, 2004). Moreover, neocortical layer I is a network layer which would exert a direct and concerted effect on the firing properties of pyramidal cells in the deep layers (Chu *et al.*, 2003; Shlosberg *et al.*, 2003). In this context, one might consider whether or not the spillover of BDNF from a certain active synapse would affect the neighbouring inactive synapses. If so, the entanglement of neuronal wires would ensue, which would be quite detrimental to neuronal function. Therefore, in order to block the leakage of neurotransmitters and other functional molecules, as well as that of BDNF, from active synapses, the astrocytes that surround active synapses may alter their morphology in response to a spillover of BDNF; in this case, astrocytes could be considered an 'insulator' of synapses. At the same time, these morphological changes among astrocytes may regulate synaptic transmission in active synapses via the release of neurotransmitters from the astrocytes themselves; in this case, astrocytes would act as an 'amplifier' of transmission (Bezzi *et al.*, 2004; Fiacco & McCarthy, 2004).

Implications of T1 and morphological changes among astrocytes and neurons in terms of adult neural plasticity

According to the current paradigm, long-term morphological changes among neurons are fundamental to learning and memory. In the present model there exists a possible mechanism for the morphological alteration of neurons and astrocytes in which BDNF–T1 signalling may also be involved.

Long-term changes in glial processes in the living brain may exert an influence on neuronal morphology. For example, the adult hypothalamo-neurohypophysial system undergoes activity-dependent morphological plasticity which modifies astrocytic coverage of its oxytocinergic neurons and their synaptic inputs. Interestingly, reduced coverage of astrocytes at synaptic sites can be maintained for 1 month by lactation (Theodosis & Poulain, 1993; Theodosis *et al.*, 2004); this finding suggests that continuous neuronal stimulation can alter as well as maintain glial morphology. In addition, such glial changes can induce morphological changes in synapses (Theodosis & Poulain, 1993; Theodosis *et al.*, 2004). In other words, a prior morphological change in the glial cells might orientate neurons with respect to sites for dendrite elongation and synapse formation. Additional studies will be needed to further clarify the changes in neuronal fine structures.

Acknowledgements

We would like to thank Dr Hans Thoenen for his helpful suggestions and comments, Dr Keiji Wada for the gift of YFP transgenic mice, and Ms Tomoko Kohno, Ms Mikako Sakurai and Ms Hiromi Fujita for genotyping of YFP mice. This work was supported by grants from the Ministry of Education, Culture, Sports, Science and Technology of Japan [no. 18700343 to K.O., no. 15016056 to M.H., nos 16200025, 17022020 and 17650100 to T.K., no. 16015341 to S.N., the Biodiversity Research of 21st Century COE (A14)] and the Organization of Pharmaceutical Safety and Research (nano-1), a Sasakawa Scientific Research Grant from The Japan Science Society, and a Core Research for Evolutional Science and Technology (CREST) grant from the Japan Science and Technology Agency (JST).

Abbreviations

BDNF, brain-derived neurotrophic factor; GFAP, glial fibrillary acidic protein; GFP, green fluorescent protein; NGF, nerve growth factor; NT, neurotrophin; S-D, Sprague–Dawley; siRNA, small interfering RNA; TrkB, tropomyosin-related kinase B; TUNEL, terminal deoxynucleotidyl transferase-mediated digoxigenin nucleotide nick-end labelling; YFP, yellow fluorescent protein.

References

Allendoerfer, K.L., Cabelli, R.J., Escanòn, E., Kaplan, D.R., Nikolics, K. & Shatz, C.J. (1994) Regulation of neurotrophin receptors during the maturation of the mammalian visual system. *J. Neurosci.*, **14**, 1795–1811.

Aloyz, R., Fawcett, J.P., Kaplan, D.R., Murphy, R.A. & Miller, F.D. (1999) Activity-dependent activation of TrkB neurotrophin receptors in the adult CNS. *Learn. Mem.*, **6**, 216–231.

Araque, A., Parpura, V., Sanzgiri, R.P. & Haydon, P.G. (2001) Tripartite synapses: glia, the unacknowledged partner. *Trends Neurosci.*, **22**, 208–215.

Armanini, M.P., McMahon, S.B., Sutherland, J., Shelton, D.L. & Phillips, H.S. (1995) Truncated and catalytic isoforms of trkB are co-expressed in neurons of rat and mouse CNS. *Eur. J. Neurosci.*, **7**, 1403–1409.

Barbacid, M. (1994) The Trk family of neurotrophin receptors. *J. Neurobiol.*, **25**, 1386–1403.

Benediktsson, A.M., Schachtele, S.J., Green, S.H. & Dailey, M.E. (2005) Ballistic labeling and dynamic imaging of astrocytes in organotypic hippocampal slice cultures. *J. Neurosci. Meth.*, **141**, 41–53.

Bezzi, P., Gundersen, V., Galbete, J.L., Seifert, G., Steinhauser, C., Pilati, E. & Volterra, A. (2004) Astrocytes contain a vesicular compartment that is competent for regulated exocytosis of glutamate. *Nat. Neurosci.*, **7**, 613–620.

Bibel, M. & Barde, Y.A. (2000) Neurotrophins: key regulators of cell fate and cell shapes in the vertebrate nervous system. *Genes Dev.*, **14**, 2919–2937.

Bushong, E.A., Martone, M.E., Jones, Y.Z. & Ellisman, M.H. (2002) Protoplasmic astrocytes in CA1 striatum radiatum occupy separate anatomical domains. *J. Neurosci.*, **22**, 183–192.

Chu, Z., Galarreta, M. & Hestrin, S. (2003) Synaptic interactions of late-spiking neocortical neurons in layer 1. *J. Neurosci.*, **23**, 96–102.

Colombo, J.A., Fuchs, E., Härtig, W., Marotte, L.R. & Puissant, V. (2000) 'Rodent-like' and 'primate-like' types of astroglial architecture in the adult cerebral cortex of mammals: a comparative study. *Anat. Embryol.*, **201**, 111–120.

Etienne-Manneville, S. & Hall, A. (2002) Rho GTPases in cell biology. *Nature*, **420**, 629–635.

Fawcett, J.P., Aloyz, R., McLean, J.H., Pareek, S., Miller, F.D., McPherson, P.S. & Murphy, R.A. (1997) Detection of brain-derived neurotrophic factor in a vesicular fraction of brain synaptosomes. *J. Biol. Chem.*, **272**, 8837–8840.

Fawcett, J.P., Bamji, S.X., Causing, C.G., Aloyz, R., Ase, A.R., Reader, T.A., McLean, J.H. & Miller, F.D. (1998) Functional evidence that BDNF is an anterograde neuronal trophic factor in the CNS. *J. Neurosci.*, **18**, 2808–2821.

Fellin, T. & Carmignoto, G. (2004) Neurone-to-astrocyte signalling in the brain represents a distinct multifunctional unit. *J. Physiol. (Lond.)*, **559**, 3–15.

Feng, G., Mellor, R.H., Bernstein, M., Keller-Peck, C., Nguyen, Q.T., Wallace, M., Nerbonne, J.M., Lichtman, J.W. & Sanes, J.R. (2000) Imaging neuronal subsets in transgenic mice expressing multiple spectral variants of GFP. *Neuron*, **28**, 41–51.

Fiacco, T.A. & McCarthy, K.D. (2004) Intracellular astrocyte calcium waves in situ increase the frequency of spontaneous AMPA receptor currents in CA1 pyramidal neurons. *J. Neurosci.*, **24**, 722–732.

Fryer, R.H., Kaplan, D.R., Feinstein, S.C., Radeke, M.J., Grayson, D.R. & Kromer, L.F. (1996) Developmental and mature expression of full-length and truncated TrkB receptors in the rat forebrain. *J. Comp. Neurol.*, **374**, 21–40.

Glenn, L.L., Hada, J., Roy, J.P., Deschênes, M. & Steriade, M. (1982) Anterograde tracer and field potential analysis of the neocortical layer I projection from nucleus ventralis medialis of the thalamus in cat. *Neuroscience*, **7**, 1861–1877.

Grutzendler, J., Kasthuri, N. & Gan, W.B. (2002) Long-term dendritic spine stability in the adult cortex. *Nature*, **420**, 812–816.

Hartmann, M., Heumann, R. & Lessmann, V. (2001) Synaptic secretion of BDNF after high-frequency stimulation of glutamatergic synapses. *EMBO J.*, **20**, 5887–5897.

Hirrlinger, J., Hülsmann, S. & Kirchhoff, F. (2004) Astroglial processes show spontaneous motility at active synaptic terminals in situ. *Eur. J. Neurosci.*, **20**, 2235–2239.

Iino, M., Goto, K., Kakegawa, W., Okado, H., Sudo, M., Ishiuchi, S., Miwa, A., Takayasu, Y., Saito, I., Tsuzuki, K. & Ozawa, S. (2001) Glia–synapse interaction through Ca^{2+}-permeable AMPA receptors in Bergmann glia. *Science*, **292**, 926–929.

Kachi, S., Oshima, Y., Esumi, N., Kachi, M., Zack, D.J. & Campochiaro, P.A. (2005) Nonviral ocular gene transfer. *Gene Ther.*, **12**, 843–851.

Klein, R., Conway, D., Parada, L.F. & Barbacid, M. (1990) The trkB tyrosine kinase gene codes for a second neurogenic receptor that lacks the catalytic kinase domain. *Cell*, **61**, 647–656.

Kohara, K., Kitamura, A., Morishima, M. & Tsumoto, T. (2001) Activity-dependent transfer of brain-derived neurotrophic factor to postsynaptic neurons. *Science*, **291**, 2419–2423.

Kondoh, T., Motooka, Y., Bhattacharjee, A.K., Kokunai, T., Saito, N. & Tamaki, N. (2000) In vivo gene transfer into the periventricular region by electroporation. *Neurol. Med. Chir. (Tokyo)*, **40**, 618–623.

Kosako, H., Amano, M., Yanagida, M., Tanabe, K., Nishi, Y., Kaibuchi, K. & Inagaki, M. (1997) Phosphorylation of glial fibrillary acidic protein at the same sites by cleavage furrow kinase and Rho-associated kinase. *J. Biol. Chem.*, **272**, 10333–10336.

Lachica, E.A. & Casagrande, V.A. (1992) Direct W-like geniculate projections to the cytochrome oxidase (CO) blobs in primate visual cortex: axon morphology. *J. Comp. Neurol.*, **319**, 141–158.

Langle, S.L., Poulain, D.A. & Theodosis, D.T. (2003) Induction of rapid, activity-dependent neuronal-glial remodeling in the adult rat hypothalamus *in vitro*. *Eur. J. Neurosci.*, **18**, 206–214.

Lund, J.S. & Wu, C.Q. (1997) Local circuit neurons of macaque monkey striate cortex. IV. Neurons of laminae 1–3A. *J. Comp. Neurol.*, **384**, 109–126.

MacDonald, J.I.S., Verdi, J.M. & Meakin, S.O. (1999) Activity-dependent interaction of the intercellular domain of rat TrkA with intermediate filament proteins, the β-6 proteasomal subunit, Ras-GRF1, and the p162 subunit of eIF3. *J. Mol. Neurosci.*, **13**, 141–158.

Matsui, K., Jahr, C.E. & Rubio, M.E. (2005) High-concentration rapid transients of glutamate mediate neural-glial communication via ectopic release. *J. Neurosci.*, **25**, 7538–7547.

Middlemas, D.S., Lindberg, R.A. & Hunter, T. (1991) trkB, a neural receptor protein-tyrosine kinase: evidence for a full-length and two truncated receptors. *Mol. Cell. Biol.*, **11**, 143–153.

Miller, R.H. & Raff, M.C. (1984) Fibrous and protoplasmic astrocytes are Biochemically and developmentally distinct. *J. Neurosci.*, **4**, 585–592.

Ohira, K., Funatsu, N., Nakamura, S. & Hayashi, M. (2004) Expression of BDNF and TrkB receptor subtypes in the postnatal developing Purkinje cells of monkey cerebellum. *Gene Expr. Patterns*, **4**, 257–261.

Ohira, K. & Hayashi, M. (2003) Expression of TrkB subtypes in the adult monkey cerebellar cortex. *J. Chem. Neuroanat.*, **25**, 175–183.

Ohira, K., Homma, K.J., Hirai, H., Nakamura, S. & Hayashi, M. (2006) TrkB-T1 Regulates the RhoA signaling and actin cytoskeleton in glioma cells. *Biochem. Biophys. Res. Commun.*, **342**, 867–874.

Ohira, K., Kumanogoh, H., Sahara, Y., Homma, K.J., Hirai, H., Nakamura, S. & Hayashi, M. (2005a) A truncated tropo-myosine-related kinase B receptor, T1, regulates glial cell morphology via Rho GDP dissociation inhibitor 1. *J. Neurosci.*, **25**, 1343–1353.

Ohira, K., Shimizu, K. & Hayashi, M. (1999) Change of expression of full-length and truncated TrkBs in the developing monkey central nervous system. *Dev. Brain Res.*, **112**, 21–29.

Ohira, K., Shimizu, K. & Hayashi, M. (2001) TrkB dimerization during development of the prefrontal cortex of the macaque. *J. Neurosci. Res.*, **65**, 463–469.

Ohira, K., Shimizu, K., Yamashita, A. & Hayashi, M. (2005b) Differential expression of the truncated TrkB receptor, T1, in the primary motor and prefrontal cortices of the adult macaque monkey. *Neurosci. Lett.*, **385**, 105–109.

Okabe, S., Miwa, A. & Okado, H. (2001) Spine formation and correlated assembly of presynaptic and postsynaptic molecules. *J. Neurosci.*, **21**, 6105–6114.

Oliet, S.H., Piet, R. & Poulain, D.A. (2001) Control of glutamate clearance and synaptic efficacy by glial coverage of neurons. *Science*, **292**, 923–926.

Paxinos, G. & Watson, C. (1986) The rat brain in stereotaxic coordinates, 2nd Edn. Academic Press, San Diego.

Peters, A., Palay, S.L., de Webster, H. & F. (1976) *The Fine Structure of the Nervous System: the Neurons and Supporting Cells*. W.B. Saunders Co., Philadelphia, pp. 242–244.

Raff, M.C., Abney, E.R., Cohen, J., Lindsay, R. & Noble, M. (1983) Two types of astrocytes in cultures of developing rat white matter: differences in morphology, surface gangliosides, and growth characteristics. *J. Neurosci.*, **3**, 1289–1300.

Rockland, K.S. & Virga, A. (1989) Terminal arbors of individual 'feedback' axons projecting from area V2 to V1 in the macaque monkey: a study using

immunohistochemistry of anterogradely transported Phaseolus vulgaris-leucoagglutinin. *J. Comp. Neurol.*, **285**, 54–72.

Rose, C.R., Blum, R., Pichler, B., Lepier, A., Kafitz, K.W. & Konnerth, A. (2003) Truncated TrkB-T1 mediates neurotrophin-evoked calcium signalling in glia cells. *Nature*, **426**, 74–78.

Shlosberg, D., Patrick, S.L., Buskila, Y. & Amitai, Y. (2003) Inhibitory effect of mouse neocortex layer I on the underlying cellular network. *Eur. J. Neurosci.*, **18**, 2751–2759.

Theodosis, D.T., Piet, R., Poulain, D.A. & Oliet, S.H.R. (2004) Neuronal, glial and synaptic remodeling in the adult hypothalamus: functional consequences and role of cell surface and extracellular matrix adhesion molecules. *Neurochem. Int.*, **45**, 491–501.

Theodosis, D.T. & Poulain, D.A. (1993) Activity-dependent neuronal-glial and synaptic plasticity in the adult mammalian hypothalamus. *Neuroscience*, **57**, 501–535.

Tigges, J. & Tigges, M. (1985) Subcortical sources of direct projections to visual cortex. In Peters, A. & Jones, E.G. (eds), *Cerebral Cortex: Visual Cortex*, **Vol. 3**. Plenum Press, New York, pp. 351–378.

Ventura, R. & Harris, K.M. (1999) Three-dimensional relationships between hippocampal synapses and astrocytes. *J. Neurosci.*, **19**, 6897–6906.

Volterra, A. & Meldolesi, J. (2005) Astrocytes, from brain glue to communication elements: the revolution continues. *Nat. Rev. Neurosci.*, **6**, 626–640.

Wenzel, J., Lammert, G., Meyer, U. & Krug, M. (1991) The influence of long-term potentiation on the spatial relationship between astrocyte processes and potentiated synapses in the dentate gyrus neuropil of rat brain. *Brain Res.*, **560**, 122–131.

Wiesenhofer, B., Kaufmann, W.A. & Humpel, C. (1999) Improved lipid-mediated gene transfer in C6 glioma cells and primary glial cells using FuGene. *J. Neurosci. Meth.*, **92**, 145–152.

Yacoubian, T.A. & Lo, D.C. (2000) Truncated and full-length TrkB receptors regulate distinct modes of dendritic growth. *Nat. Neurosci.*, **3**, 342–349.

Yan, Q., Rosenfeld, R.D., Matheson, C.R., Hawkins, N., Lopez, O.T., Bennett, L. & Welcher, A.A. (1997) Expression of brain-derived neurotrophic factor protein in the adult rat central nervous system. *Neuroscience*, **78**, 431–448.

Zhu, Y. & Zhu, J.J. (2004) Rapid arrival and integration of ascending sensory information in layer 1 nonpyramidal neurons and tuft dendrites of layer 5 pyramidal neurons of the neocortex. *J. Neurosci.*, **24**, 1272–1279.

Development/Plasticity/Repair

Brain-Derived Neurotrophic Factor Regulates the Maturation of Layer 4 Fast-Spiking Cells after the Second Postnatal Week in the Developing Barrel Cortex

Chiaki Itami,[1] Fumitaka Kimura,[2] and Shun Nakamura[1]

[1]Division of Biochemistry and Cellular Biology, National Institute of Neuroscience, Tokyo 187-8502, Japan, and [2]Division of Neurophysiology, Osaka University Graduate School of Medicine, Osaka 565-0871, Japan

Brain-derived neurotrophic factor (BDNF) has been reported to play a critical role in modulating plasticity in developing sensory cortices. In the visual cortex, maturation of neuronal circuits involving GABAergic neurons has been shown to trigger a critical period. To date, several classes of GABAergic neurons are known, each of which are thought to play distinct functions. Of these, parvalbumin (PV)-containing, fast-spiking (FS) cells are suggested to be involved in the initiation of the critical period. Here, we report that BDNF plays an essential role in the normal development of PV–FS cells during a plastic period in the barrel cortex. We found that characteristic electrophysiological properties of PV–FS cells, such as low spike adaptation ratio, reduced voltage sags in response to hyperpolarization, started to develop around the second postnatal week and attained adult level in several days. We also found that immunoreactivity against PV was also acquired after the similar developmental time course. Then, using BDNF(−/−) mice, we found that these electrophysiological as well as chemical properties were underdeveloped or did not appear at all. We conclude BDNF regulates the development of electrophysiological and immunohistochemical characteristics in PV–FS cells. Because BDNF is suggested to regulate the initiation of plasticity, our results strongly indicate that BDNF is involved in the regulation of the critical period by promoting the functional development of PV–FS GABAergic neurons.

Key words: BDNF; GABAergic neurons; parvalbumin; barrel cortex; fast spiking; critical period; local circuit

Introduction

The neurotrophin family of growth factors has been identified as being key regulatory factors for survival, neuronal differentiation, axonal as well as dendritic growth, and synaptic formation (Thoenen, 1995; Lewin and Barde, 1996). In addition to such classical roles, recent studies have revealed that neurotrophins also promote specific forms of synaptic plasticity during the postnatal period (Kovalchuk et al., 2004; Nagappan and Lu, 2005). In the visual cortex, where activity-dependent plasticity has been studied extensively, the overexpression of brain-derived neurotrophic factor (BDNF) has been shown to accelerate the critical period of plasticity (Huang et al., 1999; Fagiolini et al., 2004; Hensch, 2005). Recently, initiation of the critical period has been reported to be triggered by the maturation of the GABAergic neuronal network, especially those of parvalbumin (PV)-containing, fast-spiking (FS) GABAergic neurons that elicit $\alpha 1$ subunit-mediated responses in the postsynaptic membrane (Hensch, 2005). In fact, GABAergic neurons are highly heterogeneous groups of cells and are classified into subpopulations, each of which appear to be implicated in specific functional roles (Kawaguchi and Kubota, 1997; Markram et al., 2004). BDNF-overexpression mice have been reported to have increased numbers of PV cells, but it was not clear how physiological properties of PV cells develop normally and how they are regulated by BDNF, which seems to be quite relevant to the observed acceleration of the critical period by an excess of BDNF (Huang et al., 1999). Another sensory cortical area that also exhibits activity-dependent plasticity with the critical period is the rodent barrel cortex, where the early critical period for thalamocortical synapses lasts until the first postnatal week, which is then followed by another plastic period for intracortical synapses in layer 4 and/or layer 4–2/3 connections (Stern et al., 2001; Bender et al., 2003). Such "late" plasticity is primarily supposed to underlie the use-dependent change of cortical representation, or map plasticity for whiskers (Feldman and Brecht, 2005). Thus, it is of particular interest to understand whether BDNF has any regulatory effect on the maturation of FS neurons, specifically whether BDNF promotes the acquisition of electrophysiological and/or chemical characteristics and, if so, at what stage of development. Might this be related to known plastic periods? To answer these questions, we first identified the normal development of several properties of FS cells that are innervated from the thalamus in layer 4 and then compared them with BDNF(−/−) mice. We found that

Received Aug. 3, 2006; revised Jan. 22, 2007; accepted Jan. 23, 2007.

This work was supported by grants-in-aid for scientific research on priority areas (C.I., F.K.), for young scientists (C.I.), and for science research (S.N.); the Japan Society for the Promotion of Science (S.N.); The Ministry of Education, Culture, Sports, Science, and Technology (S.N.); and health science research grants (nano-1) (S.N.). We thank Drs. Yoshinori Sahara, Makoto Yokosuka, and Kanae Osaki for technical advice on the protocols for staining and members of the Nakamura laboratory for helpful discussions.

Correspondence should be addressed to Dr. Chiaki Itami, Department of Physiology, Faculty of Medicine, Saitama Medical University, 38 Morohongo, Moroyama, Saitama 350-0495, Japan. E-mail: chiaki@saitama-med.ac.jp.

DOI:10.1523/JNEUROSCI.3345-06.2007

 0270-6474/07/272241-12$15.00/0

electrophysiological and chemical properties of thalamorecipient FS cells attain maturation around the second postnatal week and BDNF is required for its maturation, thus providing evidence that BDNF regulates functional map plasticity throughout the maturation of FS GABAergic neurons.

Materials and Methods

Animals. The experimental protocols were approved by the Ethics Review Committee for Animal Experimentation of the National Institute of Neuroscience. A line of BDNF(−/−) mice was maintained on a C57BL/6J genetic background by heterozygote males, which were backcrossed onto the C57BL/6J females continuously at least seven generations before homozygotes were produced. BDNF(+/+) littermate mice were used as controls for all experiments (histology and electrophysiology). All experiments using the BDNF(−/−) mice phenotype were analyzed under double-blind conditions with no knowledge of genotype. Data were analyzed by a colleague who had not been informed about the phenotype analysis.

Electrophysiology. Brain slices (350–500 μm thickness) were prepared from BDNF(+/+) and BDNF(−/−) mice using a rotor slicer as described previously (Agmon and Connors, 1991; Itami et al., 2001). Mice (7–30 d old) were anesthetized deeply with Ethrane (0.9 ml/kg body weight; Abbott Labs, Abbott, IL) and decapitated. The brain was rapidly transferred to ice-cold oxygenated slicing artificial CSF (ACSF) consisting of the following (in mM): 230 sucrose, 3 KCl, 1.2 NaH_2PO_4, 10 $MgSO_4$, 26 $NaHCO_3$, and 10 glucose. Thalamocortical slices were immediately transferred to a holding chamber where they remained submerged in oxygenated recording ACSF consisting of the following (in mM): 124 NaCl, 3 KCl, 26 $NaHCO_3$, 1.3 $MgSO_4$, 2 $CaCl_2$, 1.2 NaH_2PO_4, and 10 glucose, pH 7.4 (295–305 mOsm). Slices were preincubated for at least 1 h at room temperature, and each slice was transferred to a recording chamber placed on the stage of an upright microscope (27–30°C).

Whole-cell current-clamp recordings were obtained from visually identified layer 4 barrel neurons using infrared differential interference contrast optics. Micropipettes (5–7 MΩ) were pulled from borosilicate glass capillary tubings (Sutter Instruments, Novato, CA). Patch pipette solutions contained (in mM) 105 K-gluconate, 30 KCl, 10 HEPES, 0.5 EGTA, 0.5 $MgCl_2$, 12 Na-phosphocreatine, 3 Mg-ATP, and 0.5 Na_2-GTP, pH 7.3 (295 mOsm). Responses were recorded using an Axopatch 200B amplifier (Molecular Devices, Palo Alto, CA), low-pass filtered at 5 kHz (NF Corporation, Yokohama, Japan), digitally sampled at 10 kHz, and monitored with pClamp software (Molecular Devices) running on a Pentium personal computer. To isolate neurons innervated by the thalamus, a concentric bipolar stimulating electrode was placed on the ventrobasal nucleus of the thalamus, and only recordings from cells in which thalamic stimulation was able to elicit EPSPs were used for analysis. Resting potentials were measured just after the patched membranes were ruptured. Input resistances and time constants of cells were determined by passing hyperpolarizing current pulses (duration, 500 ms) inducing voltage shifts of 6–15 mV negative to the resting potentials.

Data analysis. The spike frequency adaptation ratio was defined as the ratio of the first interspike interval divided by the average of the last three interspike intervals during a 500-ms-long spike train. Current–voltage (*I–V*) relationships were then examined at various membrane values by injecting a series of square current pulses (500 ms, −20 pA, 10 steps) to reach steady state. The amplitude of afterhyperpolarization (AHP) was measured as a voltage difference between the baseline and the first negative peak after the action potentials at the threshold, where only a single action potential was elicited by depolarizing current injection (Porter et al., 2001). Results are presented as mean ± SEM. In statistical tests, $p < 0.05$ was considered significant.

Immunohistochemistry. Mouse pups [postnatal day 4 (P4) to P30] were anesthetized deeply with Ethrane. The brains were removed, cut into a thalamocortical block (~1 cm thickness), and fixed for two overnight periods in 2% paraformaldehyde (PFA) in phosphate-buffered solution (PB; 0.2 M), followed by cryoprotection by immersion in 30% sucrose. The brains were mounted in Tissue-Tek Cryomold (Sakura Finetek Japan, Tokyo, Japan) and frozen rapidly on dry ice. Thalamocortical blocks were sectioned at a thickness of 40–50 μm on a cryostat (Leica, Wetzlar, Germany) and mounted on glass slides precoated with Vecta-Bond (Vector Laboratories, Burlingame, CA). The sections were washed in Tris-buffered saline (TBS; 30 mM Tris-HCl, pH 7.4, 150 mM NaCl, and 0.1% Tween 20), incubated in blocking solution (4% normal goat serum and 1% bovine serum albumin in TBS) for 90 min at room temperature, and incubated for two overnight periods at 4°C with the primary antibody. The antibodies used were rabbit anti-PV (1:5000; Swant, Bellinzona, Switzerland) and rabbit anti-calbindin D-28k (CB; 1:5000; Swant). After rinsing with TBS, the sections were incubated for 2 h at room temperature with a biotinylated secondary antibody (1:200, goat anti-rabbit; Vector Laboratories), which was then followed by the ABC procedure (ABC elite kit; Vector Laboratories). Every sixth section was stained for cytochrome oxidase activity by incubating the sections in a solution containing 0.01% cytochrome *c* (Sigma-Aldrich, St. Louis, MO) and 0.05% 3,3′-diaminobenzidine (Sigma-Aldrich) in 0.1 M PB, pH 7.4, to determine the anterior and posterior boundaries of the barrel cortex.

Cell counting. To quantify the number of PV+ and CB+ cells in the somatosensory cortex, nonstereological count methods were used to compare the number of neuronal bodies stained with immunohistochemistry in BDNF(−/−) and BDNF(+/+) littermate mice. Counts were performed on digitized images obtained from thalamocortical slices as used for electrophysiology including the barrel area captured with an ORCA-ER digital camera (Hamamatsu Photonics, Hamamatsu, Japan) on an Axiophot 2 microscope (Zeiss, Jena, Germany). Immunopositive cells in the barrel cortex across all the layers were counted. Brains from three different mice for each genotype, four to five sections per animal, were analyzed. Because BDNF(−/−) mice hardly survive past P14, obtaining those animals older than P14 was quite difficult, but we had a single BDNF(−/−) mouse that survived until P19 in the past 2 years; thus, the data from that mouse were also included. Photomicrographs were obtained from randomly selected areas containing all layers of the somatosensory tissue, as well as from three different thalamocortical sections (45 μm thickness; areas used for electrophysiology), using a 40× objective. Labeled neurons were counted across all of the layers in BDNF(−/−) and BDNF(+/+) tissue at a different age. For CB counts, heavily labeled CB+ cells were quantified excluding cells in layer 2–3, because pyramidal cells also exhibit CB immunoreactivity in layer 2–3 (Alcantara et al., 1993).

Morphological identification. For immunohistochemical and morphological characterization of recorded cells, 0.5% neurobiotin was included in the pipette solutions. After whole-cell recordings, the slices containing neurobiotin-loaded cells were fixed by immersion in 4% PFA containing 0.2% picric acid in 0.2 M PB for 1 h at room temperature. This was followed by incubation in PB containing 5% sucrose and Triton X-100 (Sigma-Aldrich) for 30 min. The tissue was frozen with dry ice and thawed in PB. The slices were again incubated in PB containing 0.5% Triton X-100, frozen with dry ice, and thawed in PB to help antibodies penetrate deeper into the slice. The slices were immersed in 4% normal goat serum for 90 min and incubated in a solution for 3 d at 4°C with the rabbit polyclonal antibody against PV (1:5000; Swant). After three rinses in TBS, the slices were incubated for two overnight periods with the following secondary antibodies: anti-rabbit IgG cyanine 5 (1:200; Chemicon, Temecula, CA) and streptavidin–fluorescein (RPN 1232, 1:200; Amersham Biosciences, Piscataway, NJ). After three rinses in TBS and PBS, the slices were then embedded with FluoroGuard antifade reagent (Bio-Rad, Hercules, CA), coverslipped, and sealed with Paper Bond (Kokuyo, Osaka, Japan).

Morphological analysis. Images of the fluorescently labeled cells were obtained using a confocal laser-scanning microscope using a 60× objective (TCS-SP2; Leica). Confocal images were reconstructed by projection to an XY plane, which was then traced and exported to electronic files. The number of primary dendrites and the total number of dendritic branches were counted, which often extended out of layer 4 and reached layers 2/3 and 5 vertically (approximately <1000 mm) and neighboring barrel columns horizontally (approximately <700 mm). Total dendritic length and total axonal length were measured using NIH Image software. For statistical analysis, Student's *t* test was used. $p < 0.05$ was considered significant.

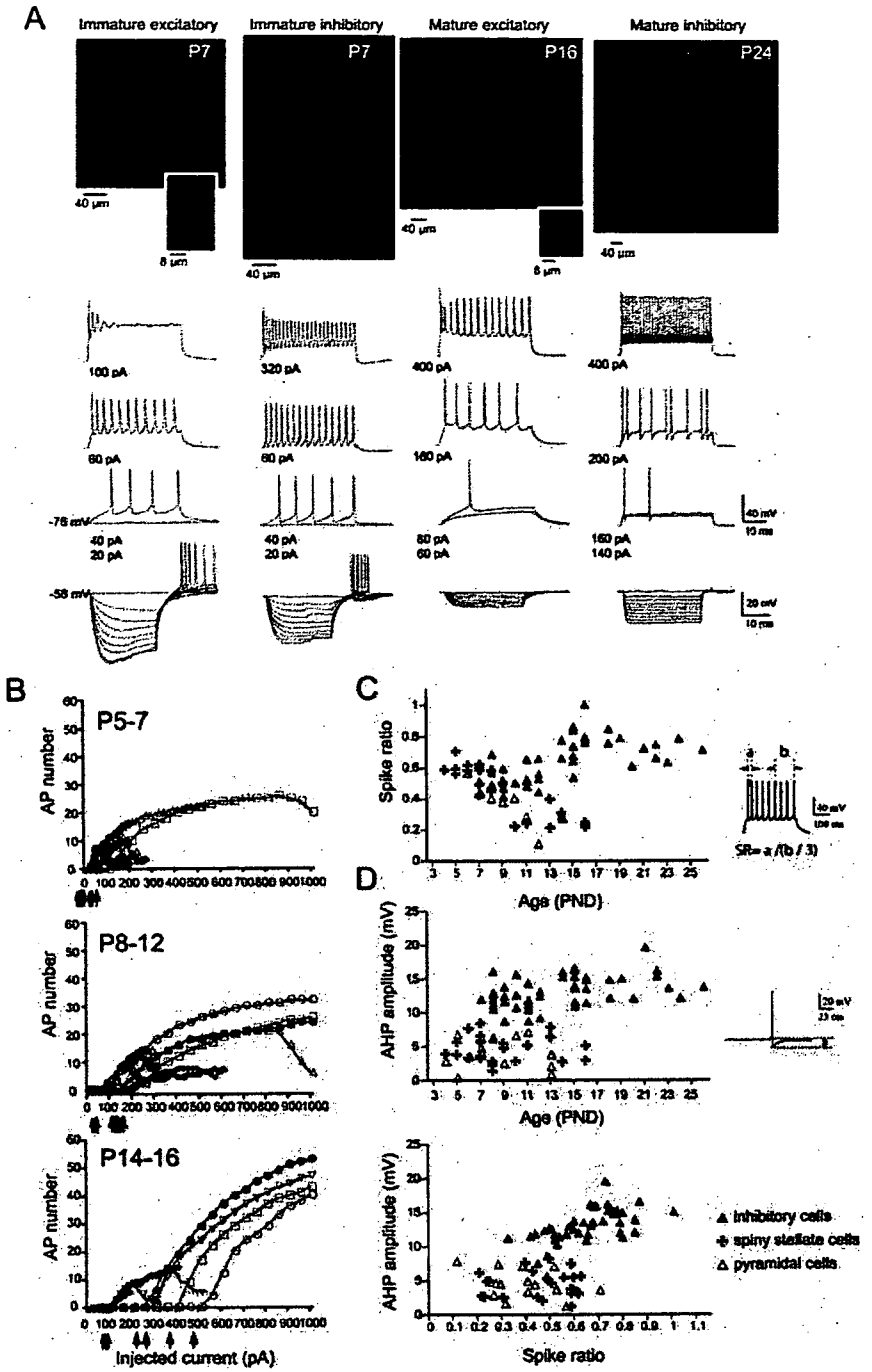

Figure 1. Morphologically identified excitatory and inhibitory cells exhibit distinct electrophysiological properties during development. ***A***, Top, Confocal photomicrograph images of representative inhibitory and excitatory neurons labeled with neurobiotin and their corresponding voltage responses to current steps. Bottom, Subthreshold, threshold, and suprathreshold responses of cells to depolarizing and hyperpolarizing current steps are shown. The amounts of currents injected are indicated on the left; hyperpolarizing current steps started at −20 pA with 20 pA decrements (duration, 500 ms). ***B***, The number of action potentials (AP) is plotted against currents injected, showing distinct profiles between excitatory (black) and inhibitory (red) cells. Excitatory cells exhibited strong adaptation, lower spike threshold, and shallower initial slopes. The latter two characteristics were remarkable especially in aged animals. ***C***, Spike frequency adaptation ratios (SR) of morphologically identified inhibitory (red triangle), spiny stellate (cross), and pyramidal (open triangle) cells in response to depolarizing current (500 ms, 500 pA) plotted against age. The inset shows the definition of SR. ***D***, ***E***, Amplitudes of AHP were plotted against age (***D***) and SR (***E***). The inset shows how we measured the amplitude of AHP. Conventions are as in ***C***. Note that all cells with an AHP amplitude >10 mV were morphologically identified as inhibitory cells. PND, Postnatal day.

Results

Electrophysiological properties that characterize inhibitory and excitatory neurons

Our first aim was to distinguish inhibitory cells from excitatory ones based on morphology and electrophysiology. For this purpose, we performed whole-cell patch recording using biocytin- or neurobiotin-filled electrodes. Recorded cells were then determined as either excitatory or inhibitory by their morphological properties (Fig. 1*A*). Those cells having spines, either exhibiting a typical pyramidal-shaped soma with apical and basal dendrites or a small round-shaped cell body with rather symmetrical dendrites, were judged as pyramidal or spiny stellate cells and designated as being excitatory cells (Saint Marie and Peters, 1985; Schubert et al., 2003). The rest were judged as inhibitory cells, which consisted of a variety of cell types such as bitufted, basket, and bipolar cells (Woolsey et al., 1975). We injected currents (depolarizing and hyperpolarizing) into each cell, and three aspects of the cellular response to the injected currents were analyzed in detail with the aim of characterizing the development of intrinsic property in cortical neurons. We first focused on the spike number in response to an increasing amount of depolarizing currents for the duration of 500 ms. Data showed that the responses of inhibitory cells were clearly distinct from those of excitatory cells throughout the development period observed by us. As shown in Figure 1*B*, inhibitory cells increased spike numbers as the injected current increased throughout the development in the present study. In contrast, excitatory cells were characterized by a sudden decrease in the number of spikes in response to injections of increasing current steps. Such a sudden reduction in spike number is referred to as "spike adaptation" or "spike accommodation." Previous studies have shown that certain kinds of K channels, such as KV3.1 and KV3.2, which are lacking or found in only small amounts in inhibitory cells, are involved in the generation of spike accommodation (Massengill et al., 1997; Martina et al., 1998). In mice older than 2 weeks of age, spike threshold and the number of spikes per injected current also helped to distinguish inhibitory from excitatory cells. Inhibitory cells needed consistently larger currents to reach spike threshold and exhibited a higher rate of spike number per injected current. This is closely related to the observation that inhibitory cells of that age

had lower input resistance than those of excitatory cells (185 ± 16 and 115 ± 9 MΩ for excitatory and inhibitory cells, respectively). Second, we examined spike adaptation ratio that was also helpful in discriminating between excitatory and inhibitory cells. The inset in Figure 1*C* illustrates the definition of spike adaptation ratio. Because the higher value of this index indicates less adaptation, we call this "spike ratio" (SR) instead of "adaptation ratio" because it is more commonly referred to. Figure 1*C* plots the SR against age for both morphologically identified excitatory ($n = 39$) and inhibitory ($n = 48$) cells. This graph clearly shows that the ratio decreased [negatively correlated with age (slope, −0.041; $r = 0.79$; $p < 0.05$)] in excitatory cells but increased slightly [positively correlated with age (slope, 0.011; $r = 0.50$; $p < 0.05$)] in inhibitory cells beyond P10. Finally, we studied the amplitude of AHP. Excitatory and inhibitory cells were reported to exhibit characteristic AHPs. Inhibitory cells have a fast sharp AHP; some inhibitory cells have additional complex components, whereas excitatory cells have a slower AHP with smaller amplitude sometimes preceded by a fast AHP, but with smaller amplitude (Porter et al., 2001; Beierlein et al., 2003). We measured the amplitude of the largest negative peak (see Materials and Methods), which occurred at 3.5 ± 3.1 ms ($n = 18$) in inhibitory cells and at 21.0 ± 6.6 ms ($n = 21$) in excitatory cells. We found that AHP was substantially larger in inhibitory cells throughout development (Fig. 1*D*,*E*). This is consistent with previous work that was performed in slightly older animals (P9–P18) (Porter et al., 2001). In their study, cells with AHPs >10 mV were all inhibitory. In our experiments, of 48 inhibitory cells, only 4 cells exhibited an AHP <10 mV (6 mV at P8, 9 mV at P9, 9 mV at P11, and 9.5 mV at P12), and conversely, all of the excitatory cells exhibited an AHP <9 mV. In conclusion, we judged recorded cells as inhibitory when they met the following criteria: (1) the number of spikes increased without sudden drop over a range of up to 1000 pA of injected current (500 pA in mice younger than P10 because young cells are less tolerant to large current); and (2) AHP was >10 mV. Using such criteria, we identified 112 cells as inhibitory from a total of 153 cells.

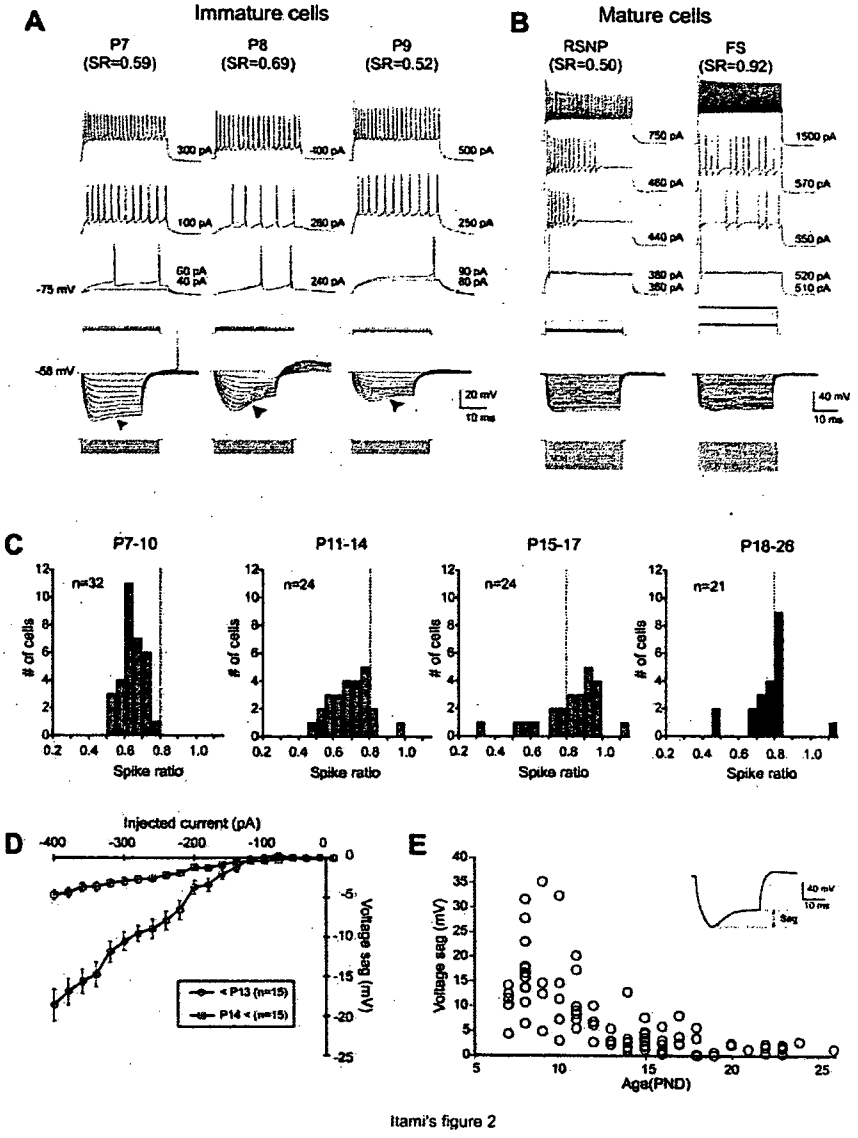

Figure 2. Developmental changes in the electrophysiological properties in inhibitory cells. ***A***, ***B***, Sample traces in response to injected currents. Three immature inhibitory cells (younger than P10) and two mature cells [regular-spiking nonpyramidal cells (RSNP), P22; FS, P15] with or without adaptation are shown. Arrowheads indicate voltage sags in response to large hyperpolarization. ***C***, SR histogram constructed from cells at four different developmental stages, showing a developmental shift toward higher values with age. FS cells (>0.8) appeared only after the second postnatal week. ***D***, *I–V* relationship of the amplitude of voltage sags in immature (younger than P13) and mature cells (older than P14). ***E***, Individual values of the amplitude of voltage sags were plotted against age. PND, Postnatal day.

Developmental changes in adaptation ratio in inhibitory cells

Inhibitory cells were further classified into two subclasses depending on the extent of adaptation (Fig. 2*B*): one exhibiting substantial adaptation (SR < 0.8) and the other exhibiting less or no adaptation (0.8 < SR). The former corresponds to regular-spiking nonpyramidal cells, and the latter corresponds to FS cells (Kawaguchi, 1995; Gibson et al., 1999; Porter et al., 2001). We next examined the development of the SR from P7 to P26. Figure 2*A* shows three examples from young animals (P7–P9), all of which exhibit more or less adapting responses. Detailed analysis revealed that before P10, none of the cells had an SR >0.8. Consequently, there are no FS cell ($n = 32$) at this age (Fig. 2*C*, left), as far as we could tell from the cell population studied. Nonadapting cells were first encountered at P14. The fraction of adapting cells increased thereafter (Fig. 2*C*). We also found that immature cells often showed voltage sag in response to a large hyperpolarizing current (Fig. 2*A*, arrowheads), the amplitude of which decreased with age. Figure 2*D* compares the amplitude of voltage sag in young (younger than P13; slope, 20

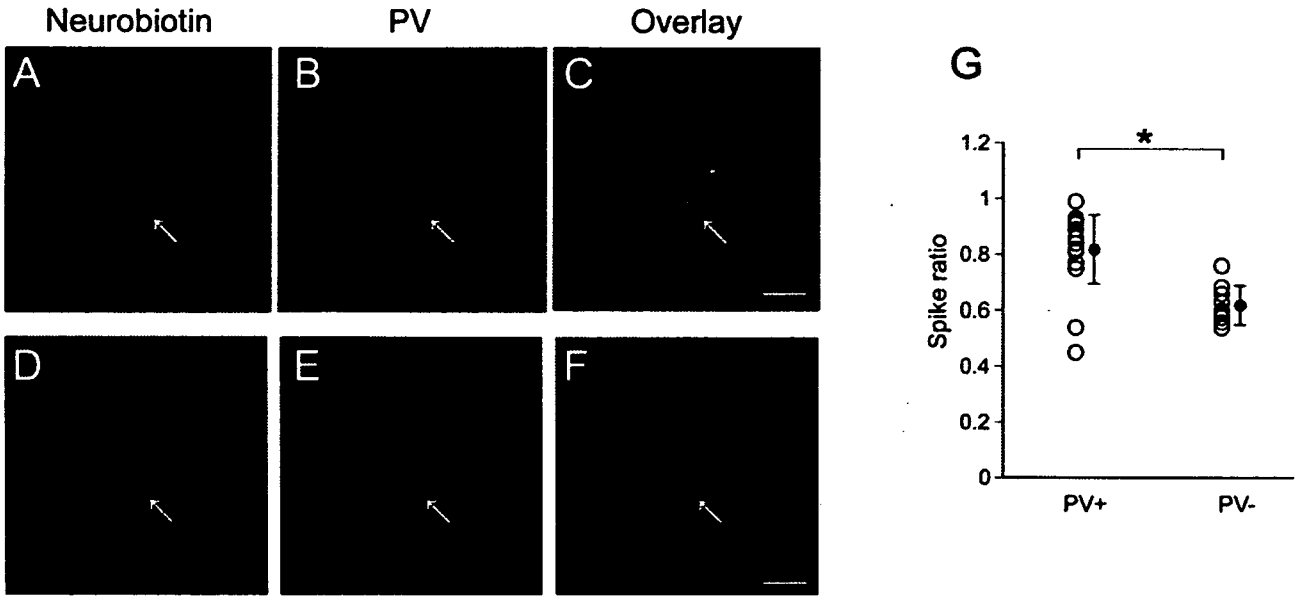

Figure 3. PV immunoreactivity was associated with a high SR. *A–F*, Identification of PV immunoreactivity in the recorded cells. *A–C*, An example of neurobiotin image, stained by FITC-conjugated avidin (*A*), which turned out to be PV immunopositive (*B*), is shown by overlaying *A* and *B* (*C*). *D–F*, An example of a PV-immunonegative cell. Staining with neurobiotin (*D*) and PV antibody (*E*) and an overlay of *D* and *E* (*F*) are shown. *G*, SRs of PV-positive and -negative cells. PV-positive cells had significantly higher SRs than those of PV-negative cells. Each symbol represents a single cell (PV+, $n = 21$; PV−, $n = 9$). *$p < 0.05$, unpaired *t* test.

mV/300 pA; $n = 15$) and aged (older than P14; slope, 3 mV/300 pA; $n = 15$) animals. The same tendency can be clearly observed in Figure 2*E*, where amplitudes of voltage sag in individual cells were plotted against age.

Developmental changes in the expressions of Ca-binding proteins

Cortical inhibitory neurons are subdivided into several groups according to the peptides contained (Hof et al., 1999; Markram et al., 2004). Of these, PV is reported to associate with the cells exhibiting a high SR value (Massengill et al., 1997; Rudy et al., 1999; Rudy and McBain, 2001). To confirm this, electrophysiological experiments were followed by immunohistochemical staining using an antibody against PV (Fig. 3*A–F*). We found that none of the PV-negative cells had an SR value >0.8 (Fig. 3*G*). As for the PV-positive cells, only 2 of 21 cells had SR values <0.8, and the difference was statistically significant (0.8 ± 0.03 and 0.62 ± 0.02 for PV-positive and -negative cells, respectively; $p <$ 0.01, unpaired *t* test). Thus, we confirmed that a high SR and PV immunoreactivity were associated during development in the mouse layer 4 barrel cortex.

We then asked the question as to whether the fraction of PV-immunoreactive cells increases with age and, if so, whether it goes parallel with physiological development as observed above. To answer this question, we investigated the developmental change in PV immunoreactivity (Fig. 4*A*, left), which was performed in thinner thalamocortical sections including the barrel cortex as electrophysiological experiments were performed. PV-immunopositive cells were barely seen at P7; they started to appear around P10, but only weakly. At P13, strongly immunopositive cells could be seen mainly in layer 4, and afterward they were seen across all the layers. On the other hand, CB immunoreactivity exhibited a distinct developmental profile; calbindin-positive cells were abundant at neonate (P4), but then the number of immunoreactive cells dramatically reduced until the second postnatal week (Fig. 4*A*, right). From this point, it stayed almost constant throughout P30, as clearly seen in Figure 4*B*, where immunopositive cells were counted across the layers in the barrel cortex.

Electrophysiological discrimination of excitatory and inhibitory cells in BDNF(−/−) mice

BDNF has been reported to have a crucial effect on the development of inhibitory neurons (Jones et al., 1994; Cellerino et al., 1996; Altar et al., 1997; Marty et al., 1997; Huang et al., 1999; Berghuis et al., 2004; Patz et al., 2004). Here, we attempted to investigate whether developmental aspects of electrophysiological properties, as we had seen so far, were also affected by BDNF. For this purpose, we first tested whether the criteria we used to discriminate between excitatory and inhibitory cells in BDNF(+/+) animals would still be appropriate in BDNF(−/−) mice. Thus, we basically repeated the same analysis as we showed in Figure 1, where we examined electrophysiological properties on morphologically identified excitatory and inhibitory cells in BDNF(−/−) mice. Figure 5*A* plots the number of action potentials in response to depolarizing current injection, as in Figure 1*B*, in BDNF(−/−) mice. As can be seen in this graph, we confirmed that morphologically identified excitatory cells again exhibited a sudden decrease in the number of action potentials while increasing depolarizing current injections in both age groups. Arrows in the abscissa indicate the threshold current for action potentials, which confirmed that inhibitory cells had higher thresholds in the older age group (P14–P16), as was the case in BDNF(+/+) mice (Fig. 1*B*). The SR in BDNF(−/−) mice also showed the similar tendency during development (Fig. 5*B*). There was a tendency that the ratio decreased or negatively correlated with age in excitatory cells (slope, −0.051; $r = 0.69$; $p =$ 0.12), whereas it was rather unchanged in inhibitory cells (slope, −0.0046; $r = 0.35$; $p = 0.63$). We did not see a slight increase with age in the SR as seen in the inhibitory cells from BDNF(+/+) mice (Fig. 1*C*); this point is to be analyzed further in more detail later. AHP was also analyzed in BDNF(−/−) mice and confirmed that AHP was substantially larger in inhibitory cells as in

BDNF(+/+) mice. As shown in Figure 5*C*, of the total of 22 morphologically identified inhibitory cells, only 3 cells exhibited an AHP with an amplitude of <10 mV, whereas none of the excitatory cells had an AHP >10 mV in amplitude. These experiments allowed us to conclude that the criteria used for discriminating excitatory and inhibitory cells in BDNF(+/+) mice could still be appropriate in BDNF(−/−) mice.

Delayed maturation of electrophysiological properties in BDNF(−/−) mice

Because in the BDNF(−/−) mice we failed to observe a slight increase in the SR (Fig. 5*B*) that was seen in BDNF(+/+) mice (Fig. 1*C*), we suspected that BDNF might have some effect on the development of the SR. As shown in Figure 6*A*, the overall shape of the distribution histogram of the SR obtained from BDNF(−/−) mice looked similar to that of the BDNF(+/+) animals. However, the cumulative histogram (Fig. 6*A*, right) indicated that a smaller fraction of cells showing higher values of the SR were in the BDNF(−/−) mice. A Kolmogorov–Smirnov test confirmed that the two distributions were significantly different ($p < 0.05$). Because cells with higher SR values started to appear around the second postnatal week (Fig. 2*C*), the difference may become apparent only after the second postnatal week. To test this, we compared cumulative curves of both BDNF(+/+) and BDNF(−/−) mice at three different developmental stages (P7–P10, P11–P14, and P15–P17). In BDNF(+/+) mice (Fig. 6*B*, left), we found that only the P15–P17 group was statistically different (Kolmogorov–Smirnov test, $p < 0.05$) from the remaining two groups, whereas in BDNF(−/−), the P15–P17 curve was not significantly different (Kolmogorov–Smirnov test, $p > 0.05$). An age-matched comparison between BDNF(+/+) and BDNF(−/−) also confirmed that the difference was only seen at P15–P17 (Fig. 6*C*). This result demonstrated that cells with higher SR values appeared after around the second postnatal week in BDNF(+/+)but not in BDNF(−/−) mice. Because BDNF(−/−) mice barely survive past the second postnatal week, we were unable to determine whether those cells were doomed not to appear or were only developmentally delayed.

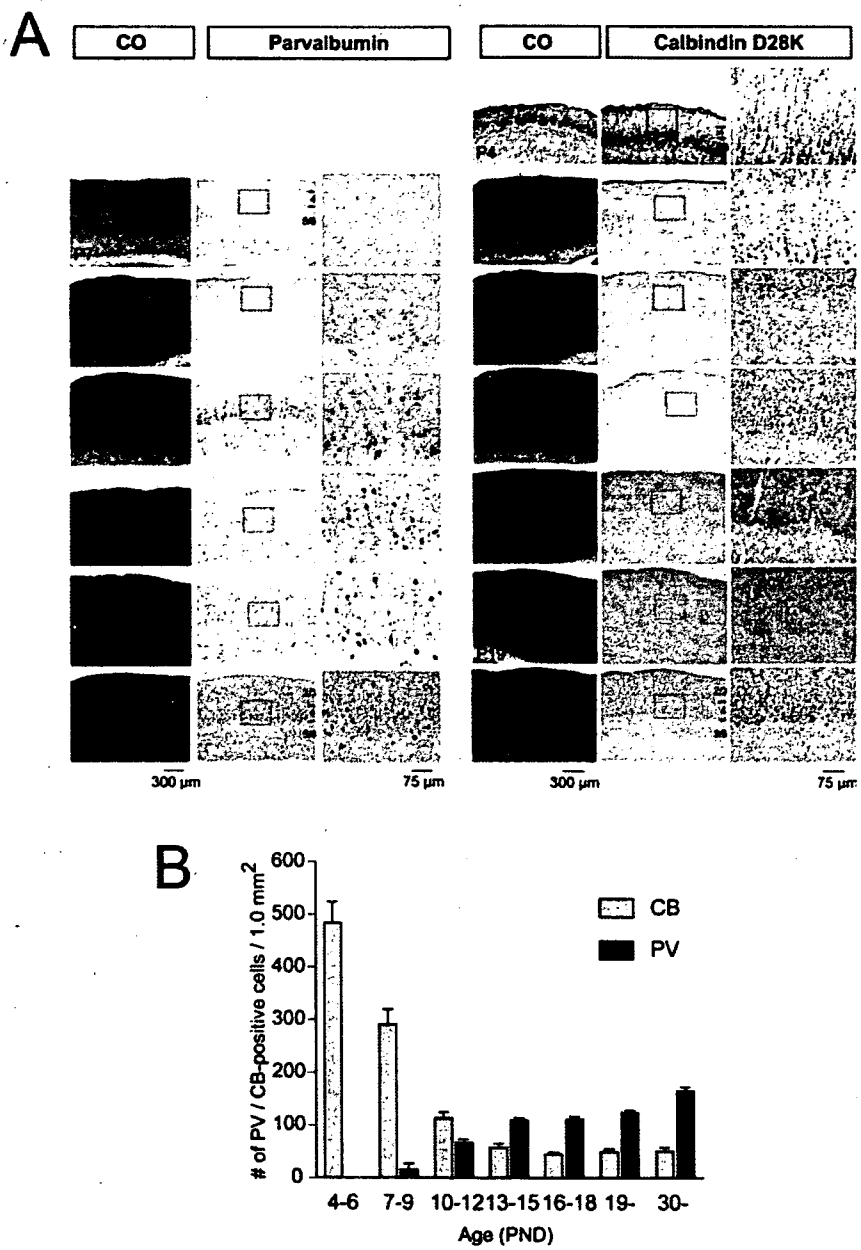

Figure 4. Strong staining of PV started to appear at P13 in layer 4 somatosensory cortex. ***A***, Three consecutive thalamocortical sections stained with cytochrome oxidase (CO), PV, or CB antibody at various stages of the development. The PV-positive cells first appeared in lower layer 4 at P9–P10. In contrast, heavily labeled CB-immunoreactive nonpyramidal cells are found even at P4 in all cortical layers but then dramatically decreased in number around the second postnatal week. Arabic numerals denote cortical layers. Squares show higher-magnification view. ***B***, Histogram showing the density of PV+ (black bars) and CB+ (gray bars) cells in the BDNF(+/+) mice at different postnatal ages constructed from immunohistological staining of these chemical markers as shown in ***A***.

Subsequently, we examined whether BDNF had any effect on the development of the hyperpolarization-activated voltage sag. The amplitude of the voltage sag in cortical inhibitory neurons was larger in young animals (Fig. 2*D*), and analysis of the *I–V* relationship identified a slope of 20 mV/300 pA before P13, which dramatically decreased to 3 mV/300 pA after P14 (Fig. 2*C*). In BDNF(−/−) mice, voltage sag was still large at P14–P16 (slope, 15 mV/300 pA), which is almost comparable to that of BDNF(+/+) animals before P13 (Fig. 6*D*, see Fig. 2*D*). An age-matched comparison of the voltage sag in response to constant 400 pA hyperpolarizing current between BDNF(+/+) and BDNF(−/−) mice older than P7–P18 revealed that statistical significance was only seen at P15–P18, but not in age group P7–P10 or P11–P14 (Fig. 6*E*).

Delayed maturation of PV immunoreactivity in BDNF(−/−) mice

PV immunoreactivity was closely associated with a high SR (Fig. 3). Thus, we next examined whether BDNF may affect PV immunoreactivity itself (Huang et al., 1999). Figure 7*A* shows the

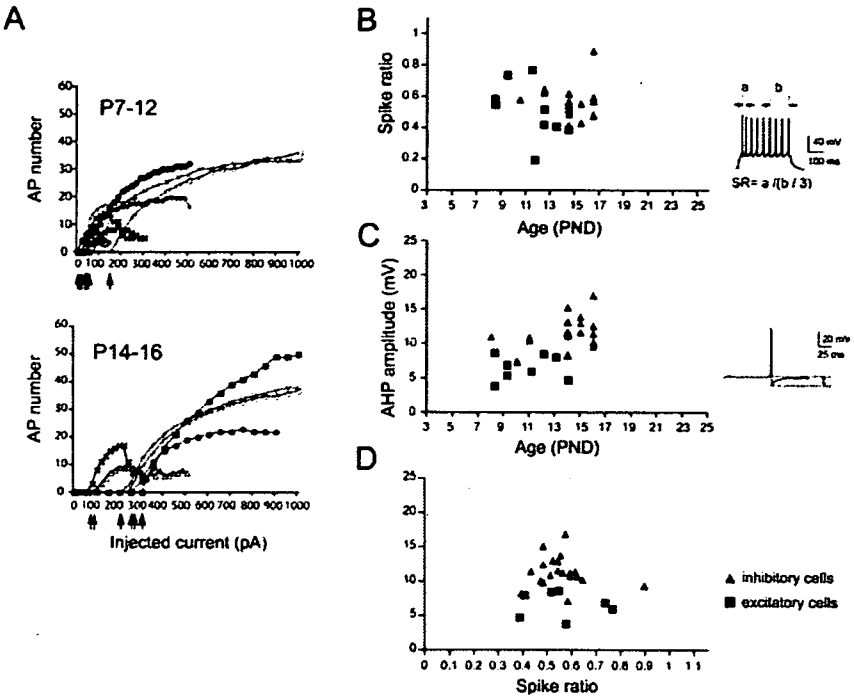

Figure 5. Distinct electrophysiological properties between excitatory and inhibitory cells in BDNF(−/−) mice. ***A***, The number of action potentials (AP) is plotted against currents injected, showing distinct profiles between excitatory (black) and inhibitory (red) cells. Excitatory cells exhibited strong adaptation and lower spike threshold. ***B***, Spike frequency adaptation ratios (SR) of morphologically identified inhibitory (red triangle) and excitatory (black square) cells in response to depolarizing current (500 ms, 500 pA) plotted against age. The inset shows how we calculated the SR. ***C***, ***D***, Amplitudes of the AHP were plotted against age (***C***) and SR (***D***). The inset shows how we measured the amplitude of AHP. Conventions are as in ***B***. PND, Postnatal day.

result of immunohistological staining of PV in BDNF(−/−) mice at four representative ages. We found that PV-positive cells did not appear before P9, and only slightly detectable staining was first observed at P10. The indication that the loss of staining before P10 was not caused by an artificial failure of staining processes, but rather to a lack of immunoreactivity of barrel cells, was obtained by strong staining of thalamic reticular (RTN) cells in the same section (Fig. 7*M*). We found that staining in RTN cells was rather constant throughout the development. Thus, we counted RTN cells in the same section, too, as an internal control for staining quality when we counted immunopositive cells in the barrel cortex across the layers. At P16 and P19, cortical layers 1–3 seemed thinner than to be expected from younger slices. In fact, BDNF has been shown to predominantly affect the development of excitatory cells, including pyramidal cells, thus altering the entire neocortical microcircuit (McAllister et al., 1995, 1999). This is consistent with previous findings (Gorski et al., 2003) using forebrain-specific BDNF knock-out mice in which they found that cortical layer 2/3 became thinner from ~3 weeks of age. They determined, however, that this was not attributable to the loss of any type of cortical cells but caused by a retraction of dendritic processes. Figure 7*Q* illustrates the quantified results of PV immunohistochemistry in the barrel cortex and RTN cells during development, where the number of positive cells in a fixed area in BDNF(−/−) mice was divided by the number of positive cells in the same fixed area in BDNF(+/+) mice in both layer 4 barrels and RTN cells. Thus, the value <1 represents a smaller number of PV-positive cells in each area in BDNF(−/−) mice. The graph clearly demonstrated that the number of PV-positive cells was smaller from P10 to P15 in BDNF(−/−) mice; or in other words, the appearance of PV-positive cells was delayed by several days, which seemed specific to the barrel area because no such delay was seen in RTN cells. A detailed comparison between BDNF(+/+) and BDNF(−/−) mice is also available in supplemental Figure 1 (available at www.jneurosci.org as supplemental material).

We have seen that the SR of BDNF(−/−) mice remained immature at P15–P17 (Fig. 6*C*, right; see also Fig. 5*B*). At this age, on the other hand, PV immunoreactivity reached levels seen in mature animals (supplemental Fig. 1, available at www.jneurosci.org as supplemental material). Such a small but clear disparity could imply that the development of SR and PV immunoreactivity proceeds independently. It would also predict that at least some of the PV-positive cells at this age might have an SR value <0.8. This prediction actually turned out to be the case, as demonstrated in Figure 8*A–G*, in which all of the PV-positive cells ($n = 6$) we examined so far had an SR <0.8, as summarized in Figure 8*G*. This result makes a clear difference from that of the BDNF(+/+) animals shown in Figure 3. Similarly, an increase in the SR and the disappearance of voltage sag seemed to develop independently, because in BDNF(−/−) mice, some cells with a high SR (>0.8) exhibited a large voltage sag (>5 mV) (Fig. 8*H*). Figure 8*I* illustrates the quantitative comparison of voltage sags in cells showing a high SR (>0.8) between BDNF(+/+) ($n = 21$) and BDNF(−/−) ($n = 5$) mice, and the difference was significant [2.7 ± 0.4 and 6.8 ± 1.8 for BDNF(+/+) and BDNF(−/−), respectively; $p < 0.01$, unpaired t test]. These results suggest that BDNF was involved in the development of PV immunoreactivity, the maturation of the SR, and the extinction of voltage sags in response to hyperpolarization but that these properties were controlled independently. We also examined whether other electrophysiological properties such as maximum spike frequency and spike threshold might be significantly different between BDNF(+/+) and BDNF(−/−) mice showing a high SR, but we did not find any significant differences in these properties (Fig. 8*J,K*).

Effect of BDNF on the morphological properties of inhibitory neurons

The electrical behavior of a given neuron has been shown to be strongly correlated with the morphology of the neuron (Kawaguchi, 2001). Thus, we next studied the effect of BDNF on the morphological properties of PV-positive cells. For this purpose, electrophysiological recordings were followed by histological staining of neurobiotin that was filled in the cell from the patch electrode. We then compared any morphological differences between BDNF(+/+) and BDNF(−/−) mice. In total, 16 neurons from BDNF(+/+) mice and 13 neurons from BDNF(−/−) mice were successfully reconstructed, 16 of which [8 each from BDNF(+/+) and BDNF(−/−)] are presented in Figure 9*A*. We counted the number of primary dendrites and dendritic branches

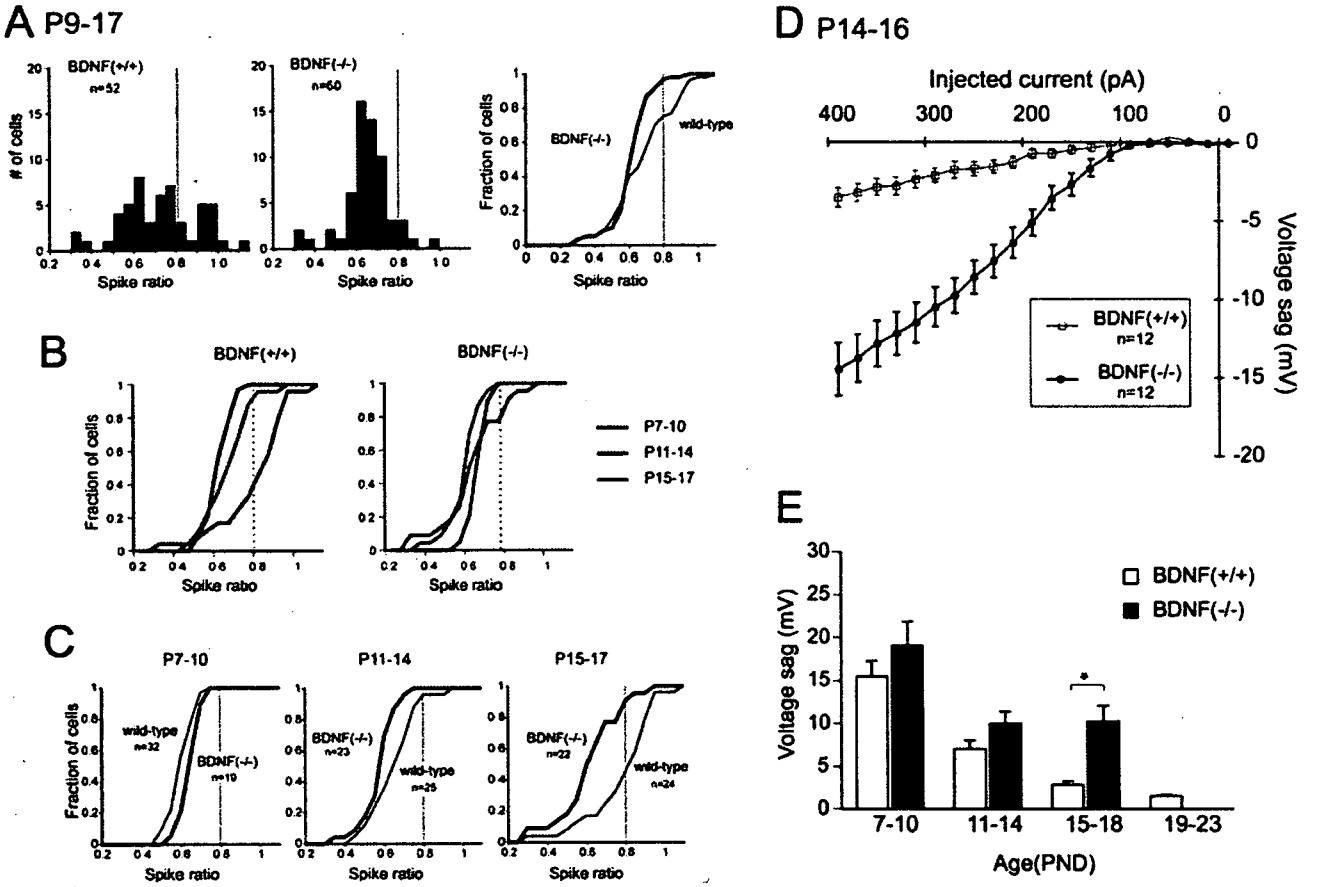

Figure 6. Immature electrophysiological characteristics in BDNF knock-outs in layer 4 inhibitory cells. *A*, Distribution histograms of SRs in inhibitory cells from P9–P17 BDNF(+/+) (left) and BDNF(−/−) (middle) mice. In the right panel, cumulative plots from BDNF(+/+) (thin line) and BDNF(−/−) (thick line) mice are superimposed. The Kolmogorov–Smirnov test indicated that the difference was significant ($p < 0.05$). *B*, Cumulative plots from BDNF(+/+) (left) and BDNF(−/−) (right) mice (Wright et al., 1997). In each graph, data were split into three age groups to show that the P15–P17 curve is shifted to the left in BDNF(+/+) animals, whereas such an age-dependent shift is not seen in BDNF(−/−) mice. *C*, For age-match comparison, the cumulative plot in *B* was further reconstructed at each age group, showing that only the P15–P17 curve is shifted to the left in BDNF(+/+) mice (left) and the rest of the two curves at P7–P10 and P11–P14 exhibited no difference. *D*, *I–V* relationship for voltage sags in BDNF(+/+) and BDNF(−/−) mice at P14–P16. *E*, Differential age-dependent changes between BDNF(+/+) and BDNF(−/−) mice in the amplitude of voltage sags in response to hyperpolarizing current (300 pA). Error bars indicate SEM. PND, Postnatal day. *$p < 0.05$, unpaired *t* test.

and measured total dendritic length and total axonal length throughout the layers in the barrel cortex. Statistical tests indicated that there were significant differences in the number of primary dendrites, total dendritic length, and the number of dendritic branches between the BDNF(+/+) and BDNF(−/−) mice (Student's *t* test, $p < 0.05$). In contrast, we failed to find a significant difference in total axonal length between the two strains.

Discussion

In the present study, we determined three main findings: (1) that electrophysiological and chemical properties of FS cells in the layer 4 barrel cortex reached nearly adult levels around the second postnatal week; (2) that these properties of FS cells were delayed in the absence of BDNF; (3) that BDNF promoted the development of dendritic arborization but not that of axons in the FS cells. Collectively, these findings indicated to us that BDNF has a pivotal role in the normal development of FS cells by acting on immature PV-positive cells. Before discussing the implications of our results, we will discuss the validity of the identification of the cell types concerned because this forms the basis of the current study.

Distinguishing inhibitory from excitatory cells by electrophysiological properties

To distinguish inhibitory interneurons from excitatory cells, we first relied on morphological characteristics. We then found that some electrophysiological features were closely associated with spike pattern as well as certain morphological characteristics. For example, morphologically identified excitatory neurons exhibited strong spike adaptation (McCormick et al., 1985; Chagnac-Amitai and Connors, 1989; Connors and Gutnick, 1990; Schubert et al., 2003), whereas inhibitory neurons were characterized by prominent AHP (Porter et al., 2001; Beierlein et al., 2003). Electrical properties such as spike adaptation and AHP are closely related to certain types of K channels expressed in each cell type (Massengill et al., 1997; Lau et al., 2000). Adaptation is dependent on a rapidly inactivating A-type K channel that is presumably encoded by the Kv4 superfamily (Kv 4.2/4.3) and is found to be abundant in excitatory cells (Martina et al., 1998). In contrast, single-cell reverse transcription-PCR experiments revealed that almost all (89%) inhibitory interneurons contained Kv3 (Kv3.1, Kv3.2) subunit transcripts that are thought to assemble together to make fast delayed rectifier K channels, which were reported to

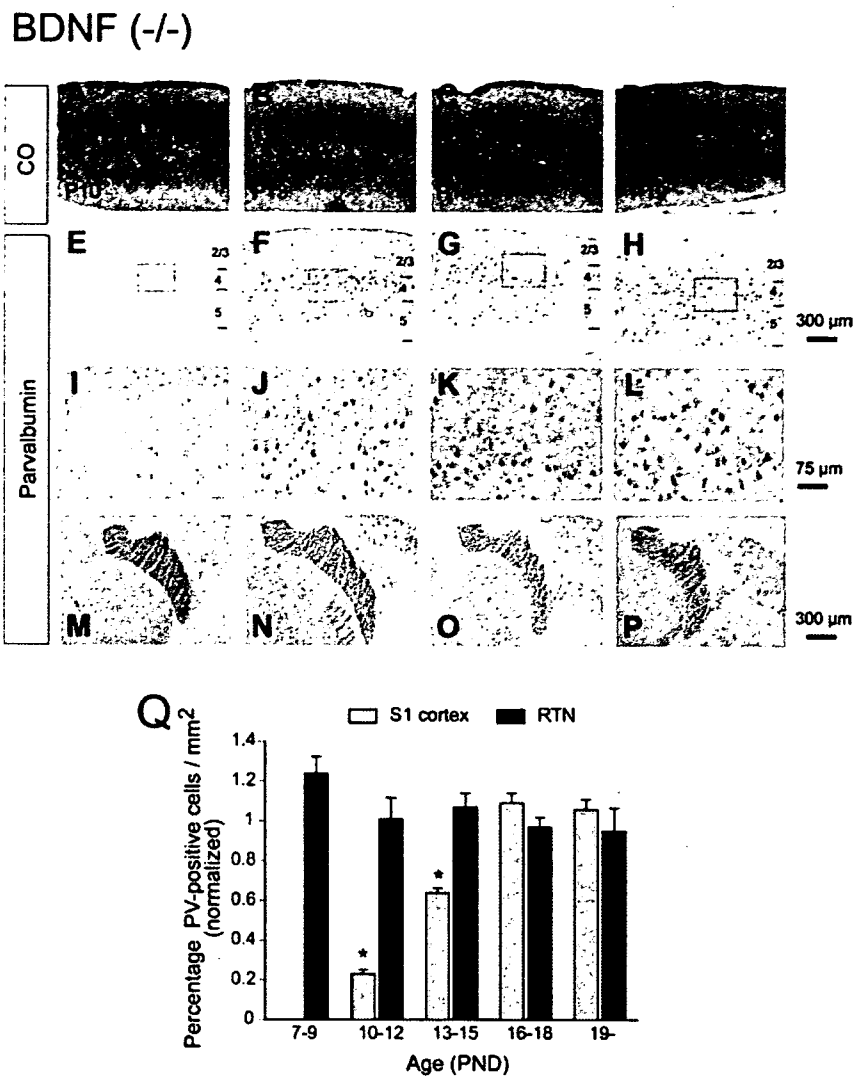

Figure 7. Delayed PV expression in BDNF knock-out mice. ***A–P***, Consecutive thalamocortical sections from P10, P13, P16, and P19 mice. Sections were stained either with cytochrome oxidase (CO; ***A–D***) or antibody against PV (***E–P***). ***E–H*** are the same magnification as ***A–D***. Squares in ***E–H*** are shown in higher magnification in ***I–L***. ***M–P***, PV staining at RTN cells in the same section as above, where PV staining was relatively consistent; thus, this area serves as an internal control for the staining in the barrel cortex. Scale bars: ***A–H***, ***M–P***, 300 μm; ***I–L***, 75 μm. ***Q***, Quantitative analysis of PV-positive cells in barrel cortex and RTN cells during development. The value was normalized with the number of positive cells in BDNF(+/+) mice by calculating the cell count in BDNF(−/−) mice divided by that in BDNF(+/+) mice. Error bars indicate SEM. *$p < 0.05$, unpaired t test.

underlie less adapting spiking behavior (Rudy and McBain, 2001; Toledo-Rodriguez et al., 2005). These channels have been shown to be present in layer 4 FS cells in the barrel cortex (Massengill et al., 1997; Chow et al., 1999). In addition, Kv3.1/Kv3.2 is also responsible for prominent AHP (Erisir et al., 1999; Lau et al., 2000). Thus, such cell type-specific distribution of particular K channels that account for two major electrophysiological characteristics such as less adaptation and AHP provides a reasonably strong logical bases on which we could rely for identification of cells either excitatory or inhibitory.

What mechanism underlies the impairment of electrophysiological properties?

We have shown that in BDNF(−/−) mice, the emergence of cells with a high SR (>0.8) was strongly suppressed after the second postnatal week (Fig. 6*B*,*C*). Moreover, we did not see extinction of the voltage sag elicited by a hyperpolarizing current (Fig. 6*D*,*E*). Voltage sag was dependent on HCN1/2 channels (Santoro et al., 2000) and was also larger in BDNF(−/−) cells at this stage of development. BDNF may regulate the function of these K channels by either trafficking these channels to or from the membrane surface (Heusser and Schwappach, 2005) or by modulating them via phosphorylation or dephosphorylation (Moreno et al., 1995). In fact, recent studies have reported that BDNF is capable of modulating the function of K channels by tyrosine phosphorylation via TrkB receptors (Tucker and Fadool, 2002). Interestingly, further study also reported that such BDNF modulation of K channels is dependent on age and previous sensory experience in the olfactory bulb (Colley et al., 2004). We have previously shown that BDNF-dependent activation of silent synapses may occur through the regulation of glutamate receptor trafficking in the thalamocortical synapses (Itami et al., 2003). Although K channels are actually subject to trafficking, it would be of great interest to assess whether BDNF could modulate the trafficking of K channels.

Effects of BDNF on dendrites versus axon

We saw a significant reduction in the number of primary dendrites, total dendritic length, and the number of dendritic branches in BDNF(−/−) compared with BDNF(+/+) mice, in addition to the previous report that BDNF has a predominant effect on the development of pyramidal neurons (McAllister et al., 1995, 1999; Horch et al., 1999). In contrast, we did not see a significant difference in total axonal length between them. This seems to indicate that BDNF has more profound effects on the development of dendrites than axons, as suggested previously (Kohara et al., 2003). This may be apparently consistent with a previous study (Gorski et al., 2003) in which they found that cortical layer 1–3 became thinner because of shrinkage of dendrites in BDNF(−/−) mice whose BDNF was deleted only in forebrain. However, because we injected dye in slice preparation with limited thickness (350–500 mm), another possible explanation might be that BDNF has more profound effects on proximal rather than distal part of neurites. Then, we might have overlooked severe effects of BDNF on distal axonal ends, at least some of which occurred out of the slices.

BDNF, GABA maturation, and relevance to plasticity in the barrel cortex

In the visual cortex, the strength of synaptic transmission among neurons can be altered or can be very plastic in an activity-

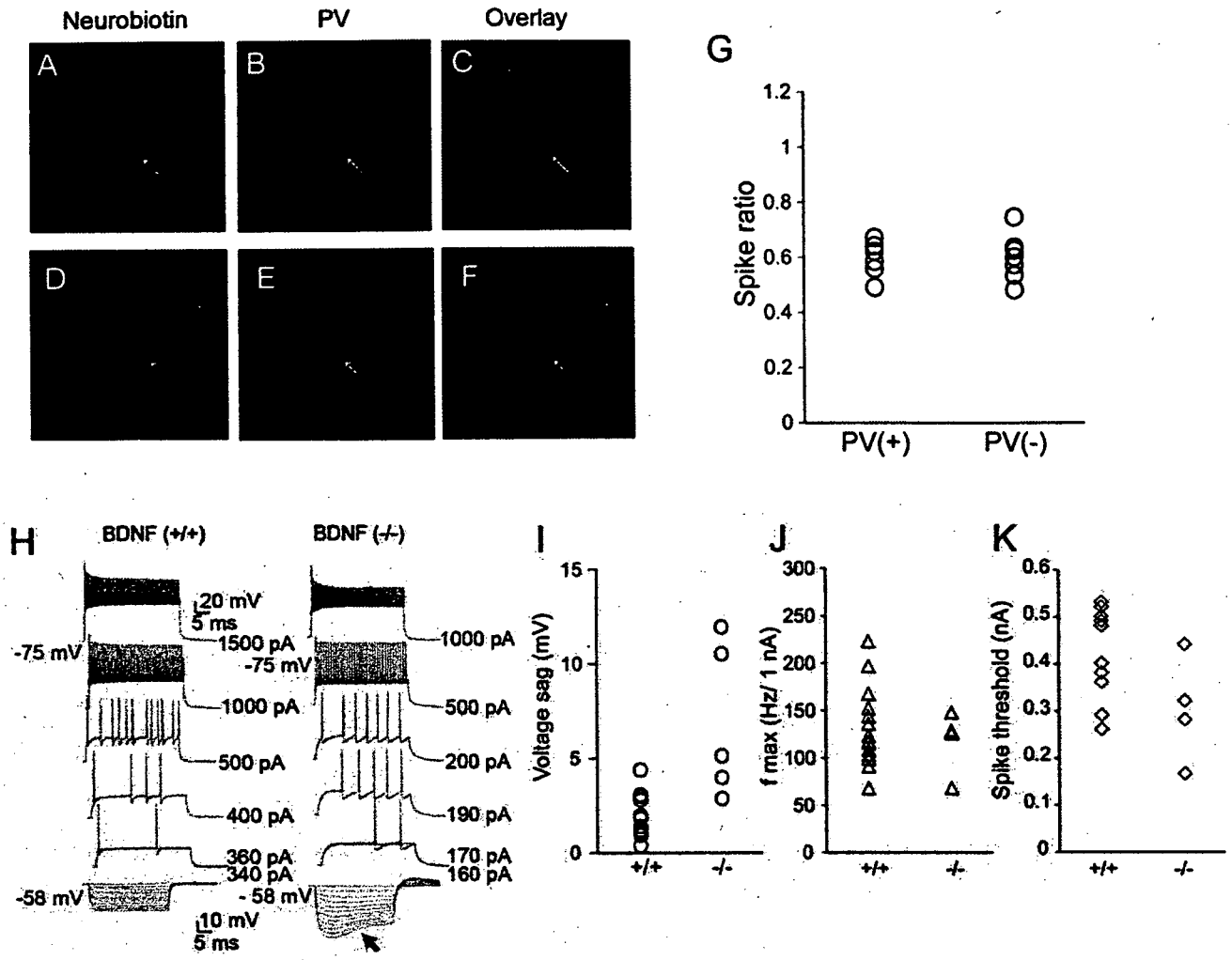

Figure 8. PV-positive cells in BDNF knock-out mice failed to show maturated electrophysiological property. ***A–F***, Examples of neurobiotin-filled inhibitory cells from BDNF(−/−) mice showing PV-immunopositive (***A–C***) or PV-immunonegative (***D–F***) staining. Neurobiotin images (***A***, ***D***), counterstaining with a PV antibody (***B***, ***E***), and an overlay of both (***C***, ***F***) are shown. ***G***, Comparison of SRs between PV-positive and -negative cells in BDNF(−/−) mice after P14 (PV+, $n = 6$; PV−, $n = 7$). Each symbol represents individual cells. ***H***, ***I***, In BDNF(−/−) mice, some cells exhibited a high SR and large voltage sag at the same time, indicating these two properties develop independently. ***H***, Examples of voltage responses to current injection in cells from BDNF(+/+) (left) and BDNF(−/−) (right) mice. Both cells had high SRs [0.91 and 0.83 for BDNF(+/+) and BDNF(−/−) mice, respectively], whereas the right cell [from BDNF(−/−) mice] showed prominent voltage sags to hyperpolarization. ***I***, Quantitative comparison of voltage sags in nonadapting cells (SR > 0.8) between BDNF(+/+) (left) and BDNF(−/−) (right) mice. ***J***, ***K***, Similarly, the maximum frequency (***J***) and spike threshold current (***K***) were compared in the nonadapting cells between BDNF(+/+) and BDNF(−/−) mice. There were no significant differences in these parameters: the maximum frequency was 147.9 ± 7.0 and 122.2 ± 15.7 Hz/nA ($p = 0.13$, unpaired t test) for BDNF(+/+) and BDNF(−/−) mice, respectively; the spike threshold current was 0.40 ± 0.02 and 0.30 ± 0.04 nA ($p = 0.063$, unpaired t test) for BDNF(+/+) and BDNF(−/−) mice, respectively.

dependent manner at a certain period of time during development, or a critical period. Recent experiments have shown that maturation of cortical GABAergic networks triggers the start of the critical period (Fagiolini et al., 2004). Meanwhile, BDNF-overexpression mice have been found to exhibit accelerated maturation of the GABAergic network, in parallel with the critical period, or precocious start and early decline of plasticity (Huang et al., 1999). Of the diverse range of GABAergic neuron types, large basket cells eliciting a1 subunit-mediated synaptic responses, or FS cells, have been shown to be responsible for the expression of plasticity (Hensch, 2005). On the other hand, the rodent barrel cortex also exhibits activity-dependent plasticity within the critical period, where projections from layer 4–2/3, or connections within layer 2/3, were suggested to be important for plasticity to occur. We provide evidence that BDNF plays an essential role in the normal acquisition of electrophysiological and chemical properties in FS GABAergic neurons in layer IV. Under the condition that secretion of BDNF in the barrel cortex is dependent on sensory inputs, our findings could suggest a role for BDNF as a possible link between sensory inputs and the maturation of GABAergic network for plasticity to occur in the barrel cortex. By what mechanism does the maturation of GABAergic cells, especially FS cells, contribute to synaptic plasticity? In the barrel cortex, spike timings of presynaptic cells in layer 4, with regard to the excitatory postsynaptic response elicited in layer 2/3, have been shown to be important in determining the direction and strength of the plasticity (Celikel et al., 2004). FS cells in layer 4 were postulated to exert feedforward inhibition on postsynaptic excitatory relay cells in layer 4 that provide excitatory inputs to layer 2/3 cells. Thus, the maturation of FS cells